3.0 Summary

This chapter describes the influence of various important process parameters such as annealing temperature and cooling rate under hydrogen atmosphere on the magnetic properties of the permalloy materials. The phase analysis, microstructural characterization and magnetic measurements were carried out by XRD, optical microscope and B-H analyser respectively. The AC magnetic properties such as induction, remanence, coercivity, peak permeability and core loss are explained as a function of field strength, temperature, frequency and cooling rate. The salient features and role of each process parameter on the magnetic properties of Ni-Fe alloys have been discussed.

3.1 Introduction

Annealing temperature and cooling rate are two important process parameters which effect the magnetic properties of permalloy materials most. With proper control of processing conditions, the magnetic properties of the permalloy materials can be controlled over wide range. Various researchers have worked to understand the role of processing parameters on the magnetic properties [1-15]. Simple methodology used here to understand the effect of processing parameter is by varying one parameter at a time and by keeping other constant.

The materials used for experiments are listed in Table 2.2 (Chapter 2) and the process parameters varied are in given in Table 2.3 (Chapter 2). The detailed experimental procedure for the phase analysis, microstructural analysis and measurement of magnetic properties is also explained in Chapter 2. To achieve the desired magnetic properties such as high permeability, low core loss and low coercivity, the materials were annealed in H_2 atmosphere. The magnetic measurements were carried out on toroid shape samples (Fig. 3.1), details of which are also given in chapter 2, as a function of annealing temperature, cooling rate and holding time.

Fig. 3.1: Toroid shaped permalloy sample

The dimensions of the toroid samples such as path length and core area [16] were calculated using

$$l = \frac{\pi(d_o + d_i)}{2} \tag{3.1}$$

where : l = (mean) magnetic path length (cm)

d_o = toroid outside diameter (cm)

d_i = toroid inside diameter (cm)

and $A = h\frac{(do - di)}{2}$ (3.2)

where, A = Core area (cm^2)

h= height of the toroidal specimen (cm)

The magnetic properties of the samples were also studied as a function of frequency since the properties are frequency dependent [16-19] and can be understood from the equations

$$P_c = \frac{N_1 f}{N_2}\int_0^T I_1(t)V_2(t)dt\,, \tag{3.3}$$

where P_c is sample core loss (watts), N_1 the number of primary turns, N_2 the number of secondary turns, f the test frequency (Hz), T the period of one cycle, I_1 the primary current (A) and V_2 the secondary induced voltage (V).

Permeability, $\mu = \frac{1}{\mu_0}\left[\frac{E}{N_1 N_2 I}\frac{do+di}{2h(do-di)}\frac{10^2}{f}\right]$

d_o = 1.0 cm, d_i = 0.6 cm, N_1= 20, N_2 = 20, I = 1 mA, $\mu_o = 4\pi X10^{-7}$ H/m

$$\mu = \frac{E}{hf}\left[3.978X10^5\right] \qquad (3.4)$$

where E is the emf generated (mV), h the thickness of the sample (cm) and f the frequency (Hz).

3.2 Influence of process parameters on structural and magnetic properties

Sample A

Fig. 3.2 shows the X-ray diffraction patterns of sample A in unannealed condition and in annealed condition at 1100°C, 1120°C, 1140°C, 1150°C and 1180°C temperature respectively. From all the X-ray diffraction patterns, we found that an austenitic single phase Ni_3Fe is formed and the crystal structure is face centered cubic (FCC), matched with the JCPDS card number 380419 [20-21]. However, some variation in the peak intensity is noticed, which is due to the different annealing temperatures. We also noticed that with annealing, the domains are mostly aligned along <200> direction. The effect of annealing temperature on the cell dimensions is also reported. The value of lattice parameter of the sample at different annealing temperature is given in Table 3.1, which shows that there is not any significant change in the lattice parameter with increase in the annealing temperature.

Table 3.1: Variation of lattice parameter 'a' as a function of temperature

Temperature (°C)	a (A^o)
1100	3.548
1120	3.548
1140	3.552
1150	3.546
1180	3.546

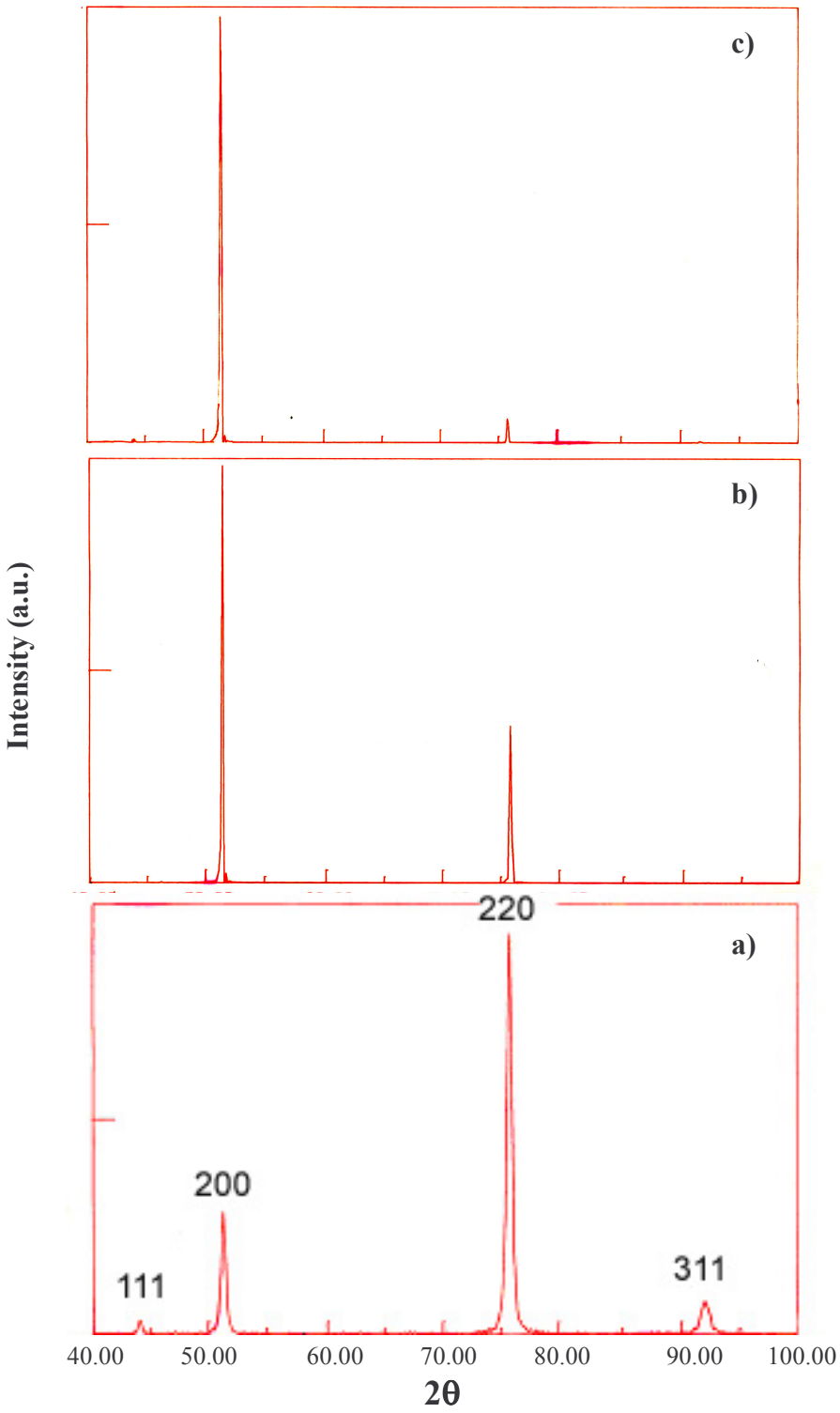

Fig. 3.2a: X-ray diffraction patterns of the sample A a) in unannealed condition, b) 1100°C and c) 1120°C

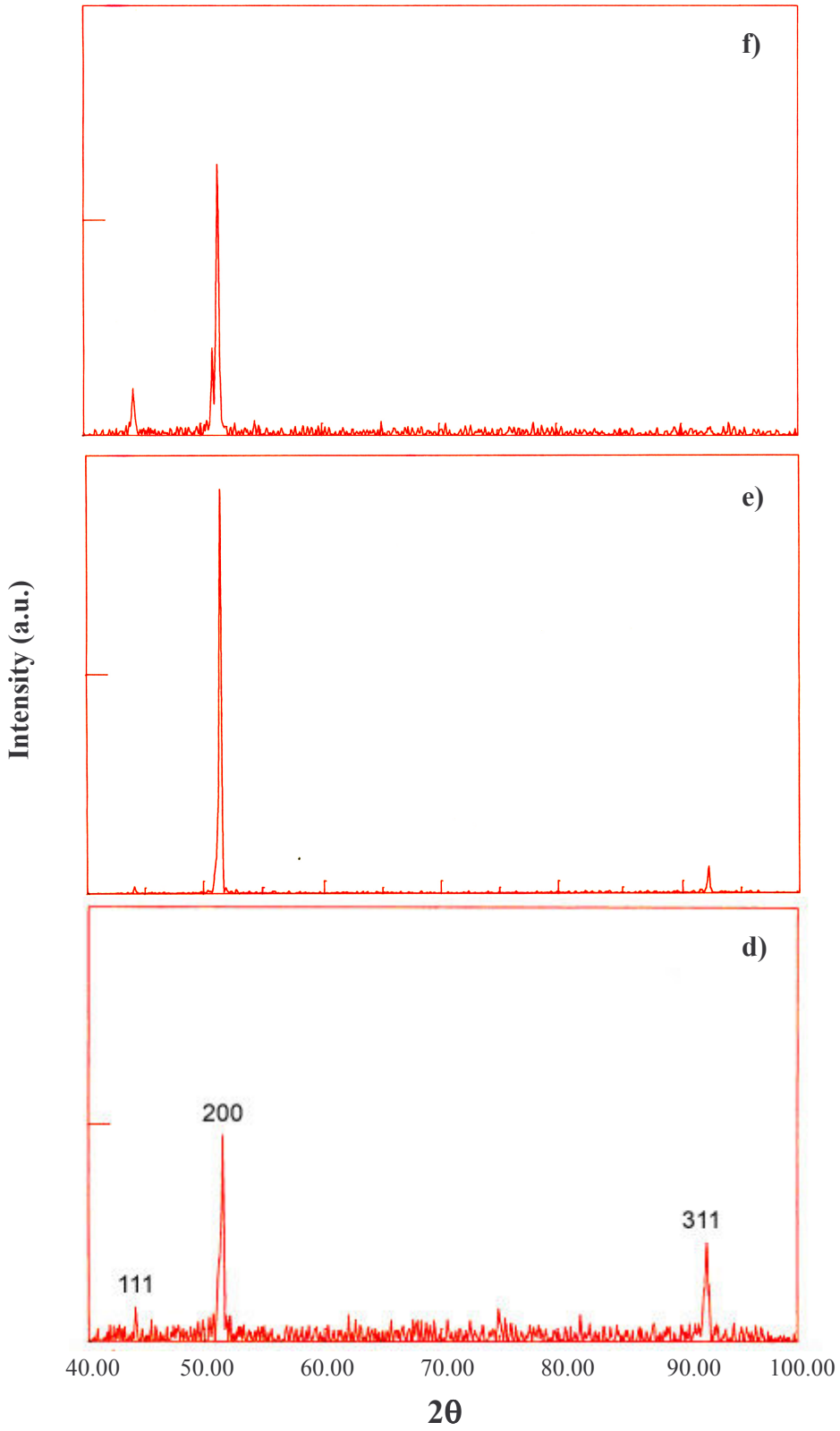

Fig. 3.2b: X-ray diffraction patterns of the sample A at d) 1140°C, e) 1150°C and f) 1180°C

Fig. 3.3 shows the optical micrographs of sample A at 100X magnification after annealed at 1100°C, 1120°C, 1140°C, 1150°C, 1160°C and 1180°C respectively. The micrographs reveal that there is not any significant grain growth in the sample A with increase in the annealing temperature. However, in all the micrographs, twin boundaries appear at the grain boundaries. The average grain diameter observed in the sample A is 320 μm.

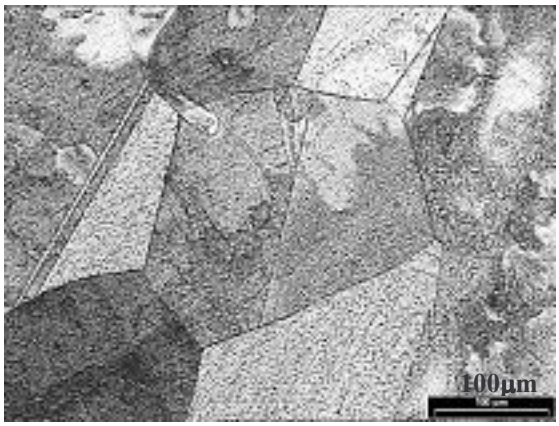

(a)

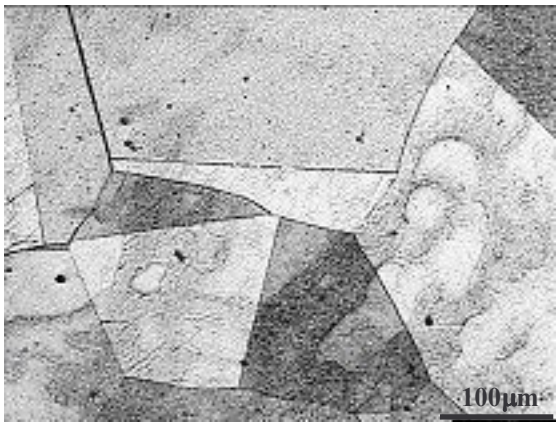

(b)

Fig. 3.3a: Optical micrographs of sample A at a) 1100°C and b) 1120°C

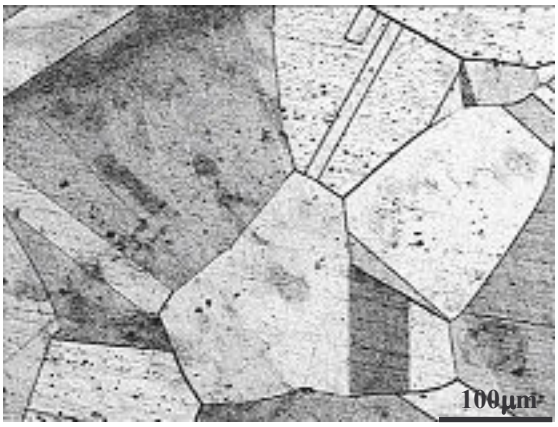

(c)

(d)

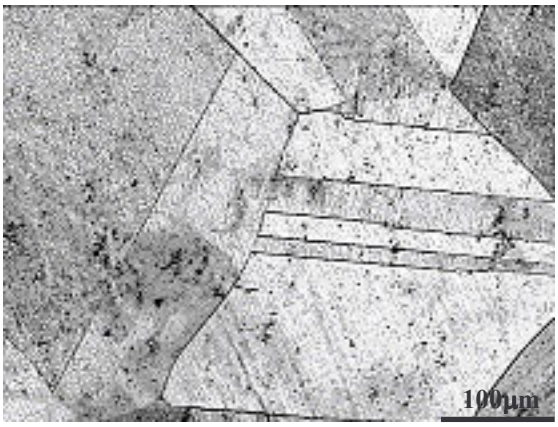

(e)

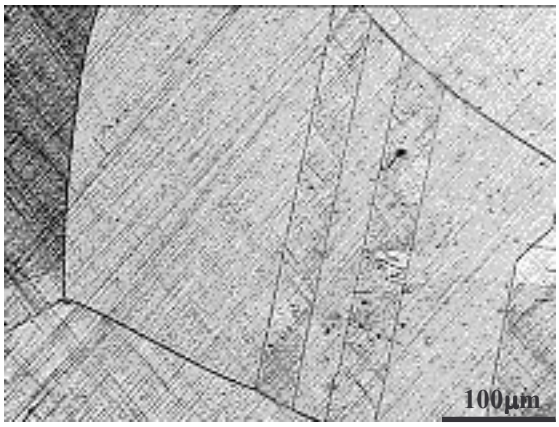

(f)

Fig. 3.3b: Optical micrographs of sample A at c) 1140°C, d) 1150°C, e) 1160°C and f) 1180°C

Table 3.2 shows the effect of the annealing temperature on the magnetic properties of sample A at 300 Hz [22].

Table 3.2: Effect of annealing temperature on magnetic properties

Annealing temperature (°C)	B_r (mT)	H_c (A/m)	Peak permeability	Core loss (mW)
1100	505.62	36.40	5581	8
1120	507.93	35.85	5577	8
1140	509.00	35.79	5796	8
1150	475.02	35.12	5525	8
1160	501.96	35.55	5640	8
1180	514.94	36.37	5628	9

Fig. 3.4 shows a typical behaviour of induction in sample A corresponding to a function of field strength. We observed that at input frequency of 300 Hz and at 1150°C, induction increases exponentially from 635 mT to about 757 mT as field strength increases from 50 A/m to 300 A/m and thereafter tends to saturate at 767 mT as the field strength is further increased to 500 A/m. Similar behaviour has been depicted at other temperatures as shown in Fig. 3.4.

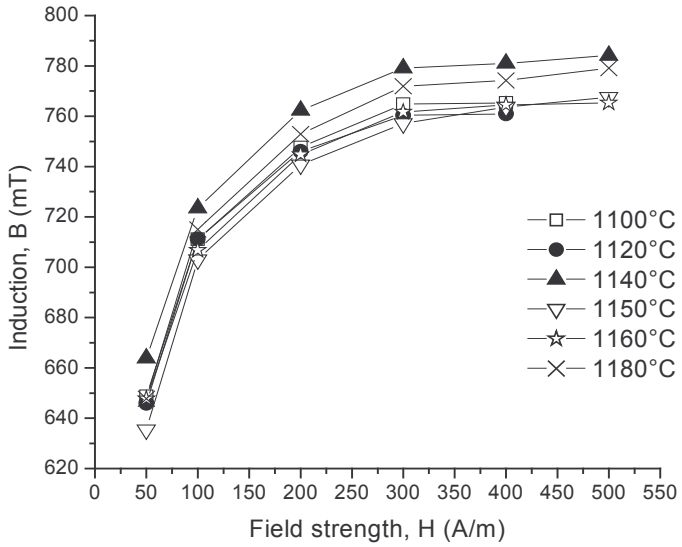

Fig. 3.4: Behaviour of induction as a function of field strength at 300 Hz

The behaviour of remanence in sample A corresponding to a function of field strength, annealing temperature, frequency and cooling rate is given in Fig. 3.5 (a-d) respectively. We observed that at an input frequency of 300 Hz, B_r increases from 465 mT to 475 mT where field strength increases from 50 A/m to 100 A/m thereafter decreases to 355 mT where the field strength increases to 500 A/m at 1150°C. Similar behaviour has been depicted at another temperatures as shown in Fig. 3.5a. The temperature dependence of B_r also shows an increase up to 1140°C temperature thereafter exponential decay at 1150°C and there after B_r increases with increase in temperature as shown in Fig. 3.5b. It is due to the field reversal, wherein the domains might tend to align opposite to initial direction. These results were reported at a constant cooling rate of 2.5°C/min. and holding time of 2 h. The behaviour of B_r is also studied as a function of frequency. We noticed that at a temperature of 1100°C, B_r increases from 429 mT to 505 mT with increase in the frequency from 100 Hz to 300 Hz as shown in Fig. 3.5c. Similar behaviour has been noticed at other temperatures. Also, B_r shows an interesting behaviour as a function of cooling rate as shown in Fig. 3.5d. The remanence decreases exponentially with increase in the cooling rate from 2 to 2.5°C/min at field strength of 100 A/m thereafter increases with increase in the cooling rate. The similar behaviour has also been seen for other field strengths. As the remanence is a structure sensitive property therefore shows changes with change in the process parameters.

The behaviour of coercivity of sample A as a function of field strength, annealing temperature, frequency and cooling rate is given in Fig. 3.6 (a-d) respectively. We observed that at an input frequency of 300 Hz and at a temperature of 1100°C, H_c increases from 24 A/m to 62 A/m as the field strength increases from 50 A/m to 500 A/m. Similar behaviour has been depicted at other temperatures as shown in Fig. 3.6a. An interesting behaviour of coercivity as a function of annealing temperature at 300 Hz frequency is shown in Fig. 3.6b. We observed that at higher field strengths i.e. 200 A/m and 400 A/m, the coercivity shows variations in the intermediate temperature range 1120°C-1160°C where as at 100 A/m the coercivity remains nearly constant indicating the stable performance of the device at this field. We noticed that at a temperature of 1100°C, the coercivity increases from 21 A/m to 36 A/m with increase in frequency from 100 Hz to 300 Hz as shown in Fig. 3.6c. Similar behaviour of coercivity has been noticed

at other temperatures. We also observed that at field strength of 100A/m, the H_c shows little variations under the lower cooling rate ranges from 2 to 3°C/min and becomes almost stable at the higher cooling rates as shown in Fig. 3.6d. Similar behaviour has been observed at other higher field strengths.

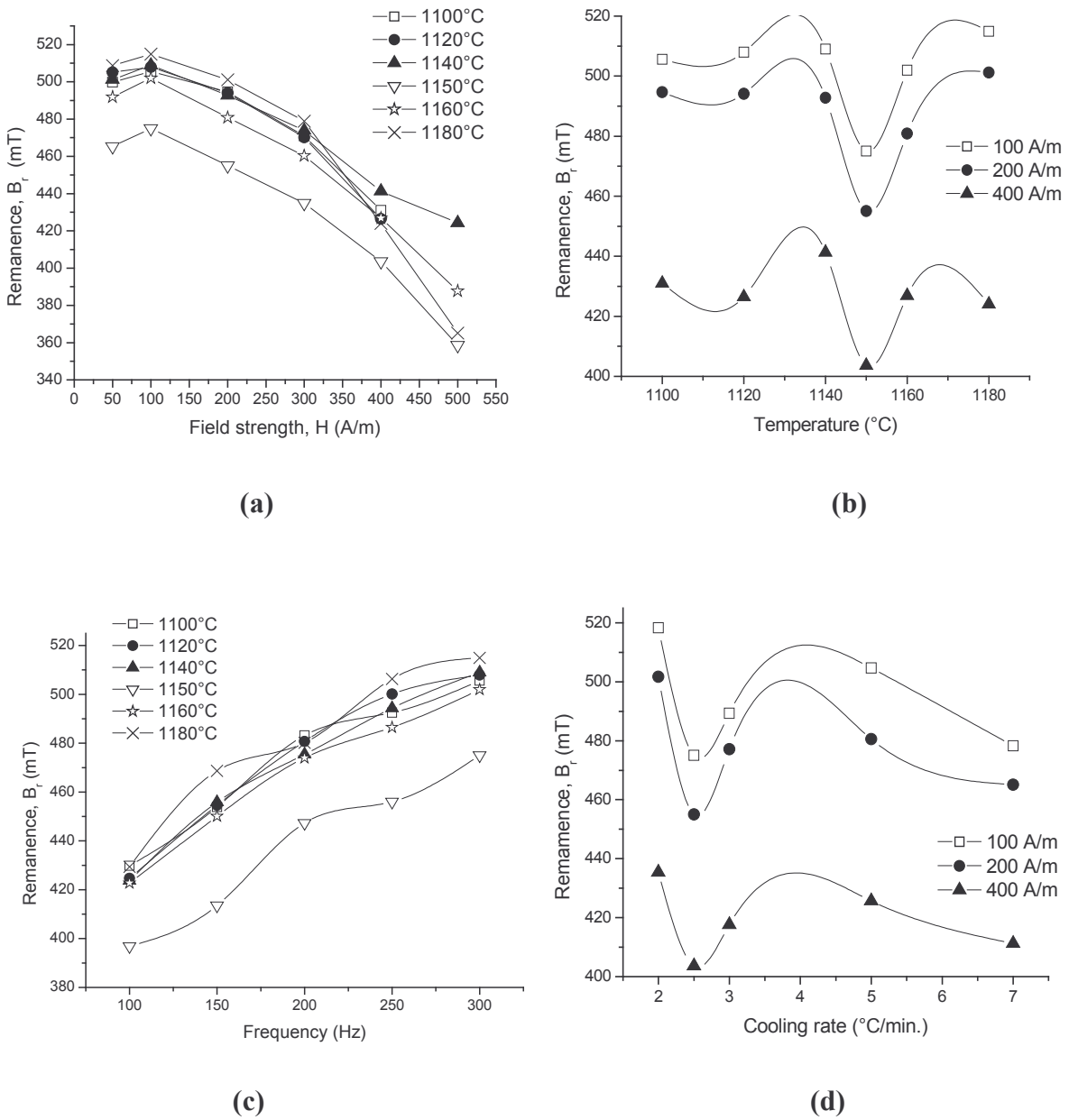

Fig. 3.5: Behaviour of remanence as a function of a) field strength, b) annealing temperature, c) frequency and d) cooling rate

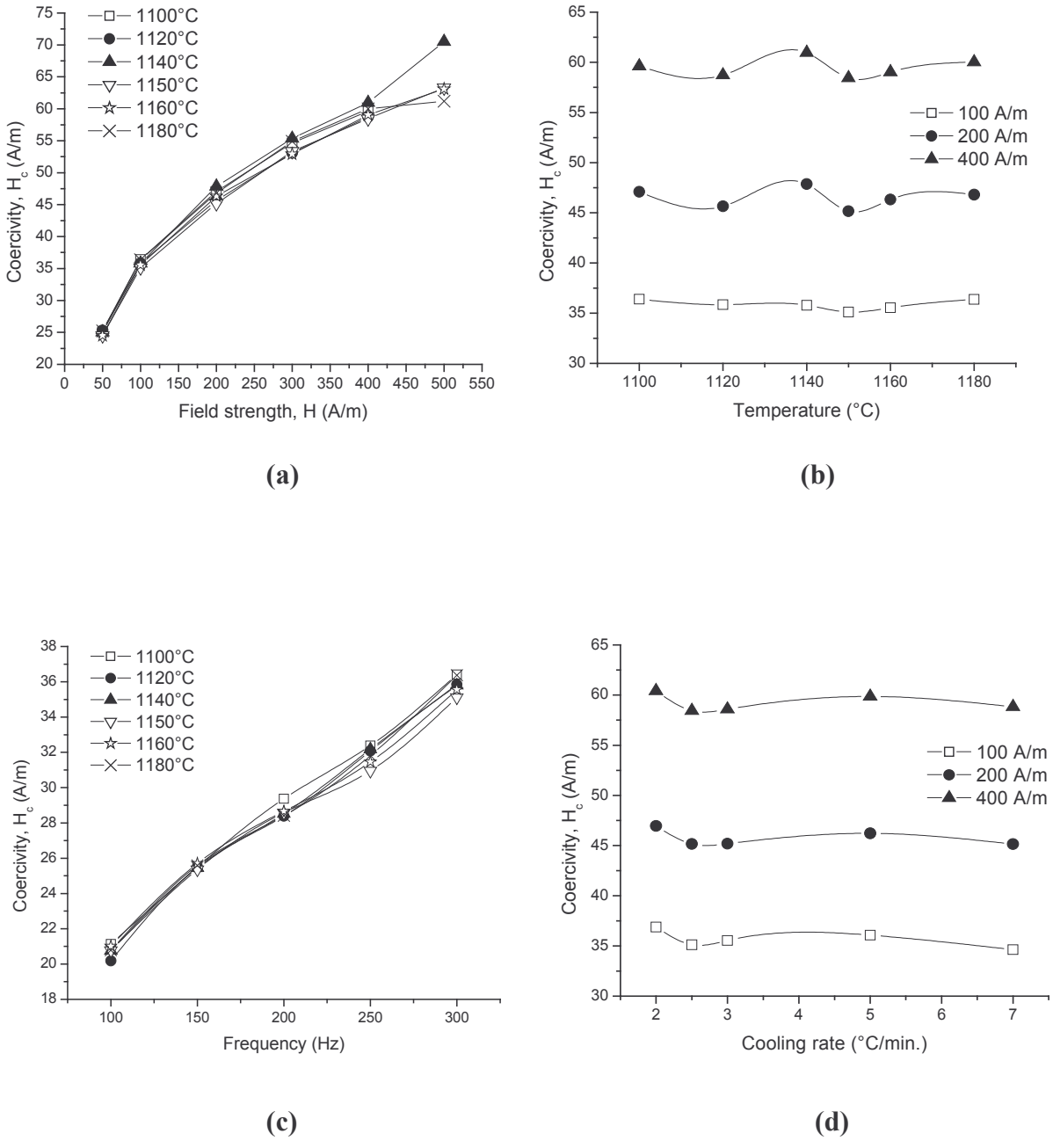

Fig. 3.6: Behaviour of coercivity as a function of a) field strength, b) annealing temperature, c) frequency and d) cooling rate

Fig. 3.7 (a-d) shows the behaviour of peak permeability as a function of field strength, annealing temperature, frequency and cooling rate respectively. We observed that at a input frequency of 300 Hz and at a temperature of 1150°C, the peak permeability decreases exponentially from 9954 to 1221 where the field strength increases from 50 A/m to 500 A/m. Similar behaviour has been depicted at other temperatures as shown in Fig. 3.7a. The temperature dependence of peak permeability shows little variation at lower field strength of 100 A/m and at input frequency of 300 Hz but shows stability at higher field strengths i.e. 200 A/m and 400 A/m as shown in Fig. 3.7b. We observed that at 1100°C temperature, the peak permeability decreases from 11268 to 9575 with increase in the frequency from 100 Hz to 300 Hz. Similar behaviour of peak permeability has been noticed at other temperatures as shown in Fig. 3.7c. This satisfies the equation 3.4, according to which the peak permeability is inversely proportional to the frequency. Also, we noticed that at higher field strengths i.e. 200 A/m and 400 A/m, the peak permeability is almost stable as function of cooling rate as shown in Fig. 3.7d. But it shows slight variations at lower field strength i.e. 100 A/m and at lower cooling rates i.e. 2 to 3°C/min.

An interesting behaviour of core loss as a function of field strength, annealing temperature, frequency and cooling rate is given in Fig. 3.8 (a-d) respectively. We observed that at 300 Hz, the core loss increases from 5 mW to 19 mW with increase in field strength from 50 A/m to 500 A/m for all studied temperatures (Fig. 3.8a). The temperature dependence of core loss shows stability at lower field strength of 100 A/m and shows variation at higher field strength for all studied temperatures as shown in Fig. 3.8b. This is due to the localized heating effect of the material at such higher field strength. The core loss is also frequency dependent as shown in Fig. 3.8c (equation 3.3). It increases from 1.4 mW to 8.9 mW with increase in the frequency form 100 Hz to 300 Hz for all studied temperatures. Also, we noticed that the core loss varies where the cooling rate increases from 2 to 3°C/min. thereafter it becomes almost stable with further increase in the cooling rate up to 7°C/min. at field strength of 100 A/m as shown in Fig. 3.8d. But the core loss shows more variations at higher field strengths. This is also due to the localized heating effect at the higher field strengths.

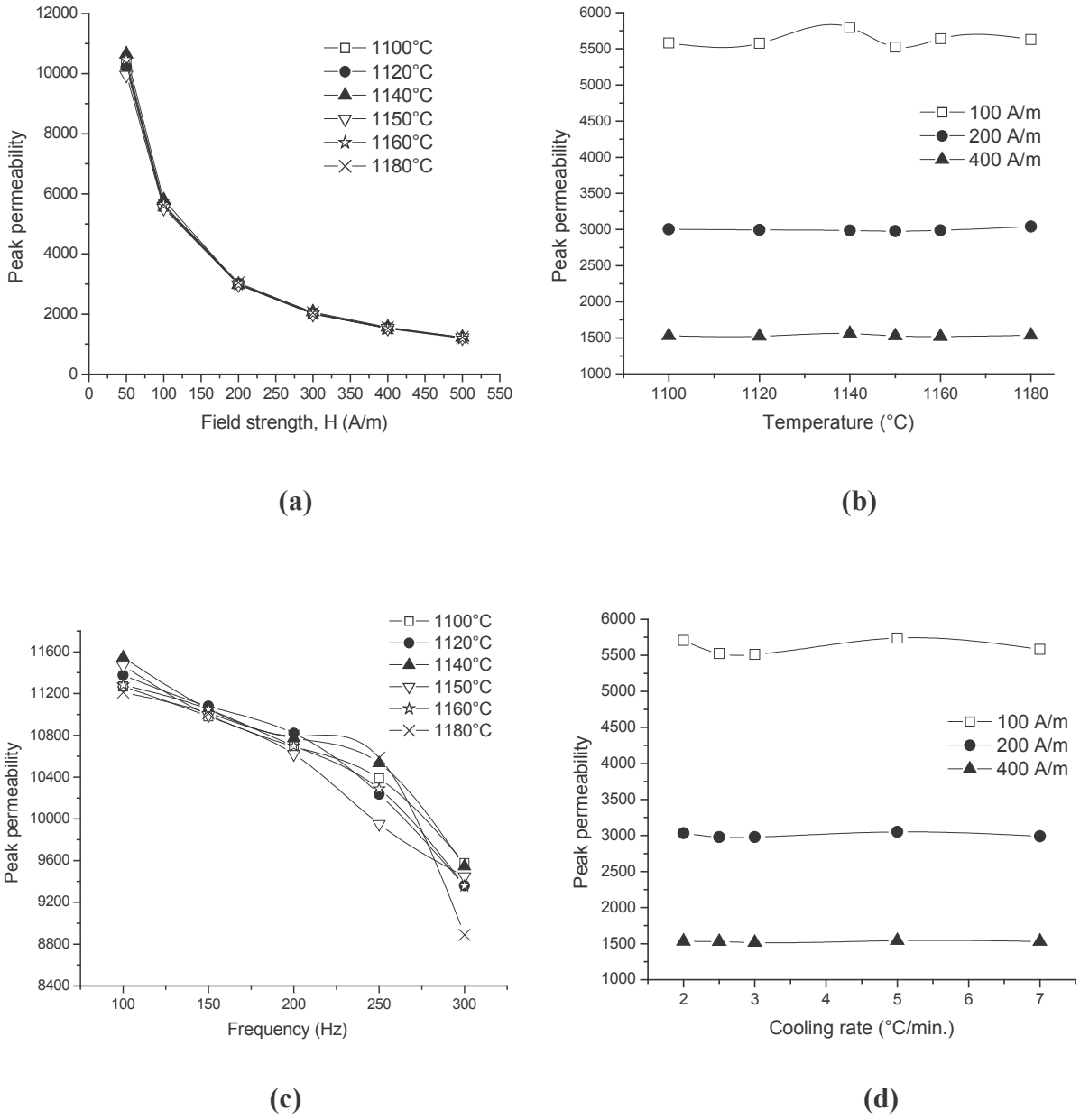

Fig. 3.7: Behaviour of peak permeability as a function of a) field strength, b) annealing temperature, c) frequency and d) cooling rate

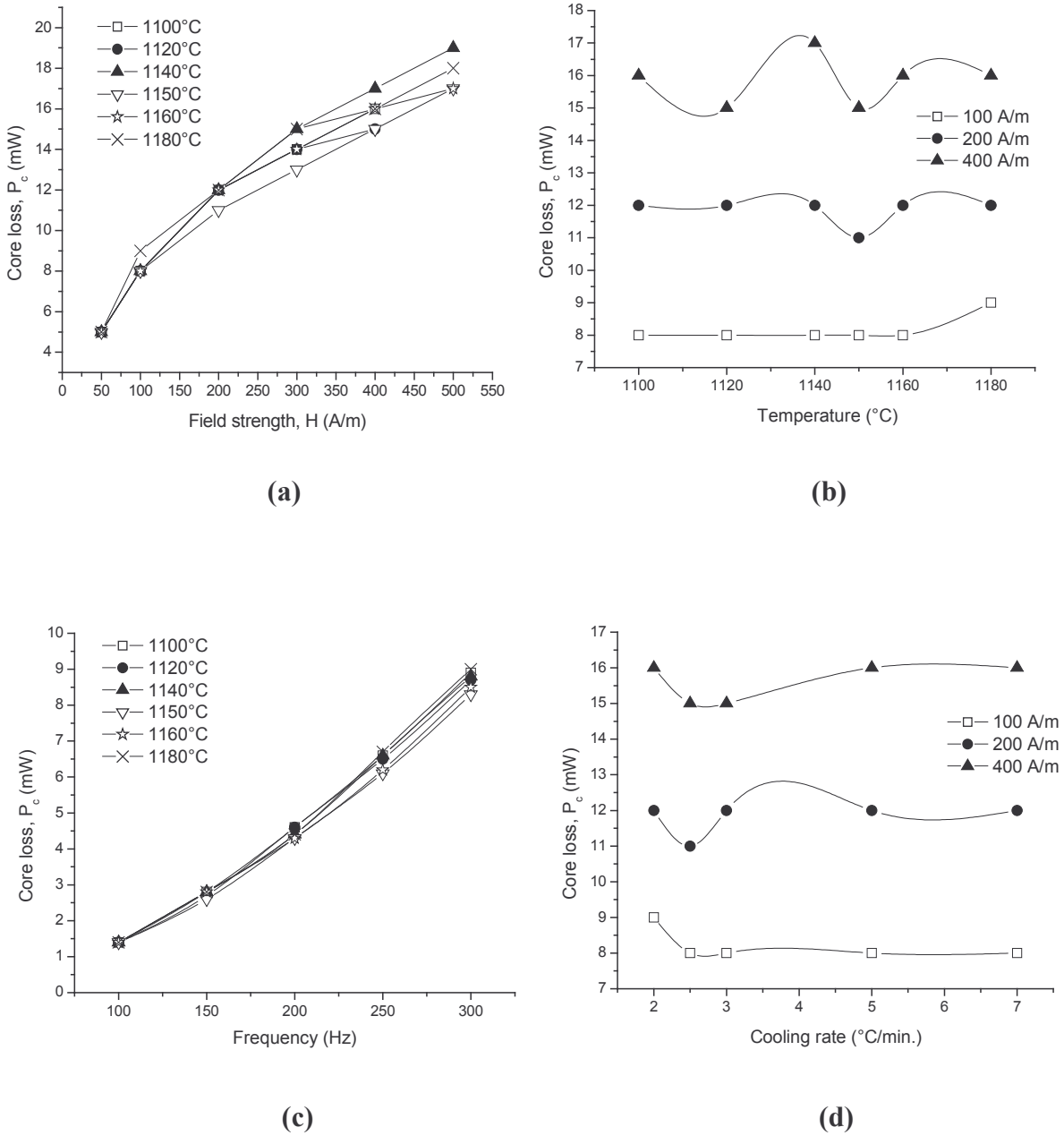

Fig. 3.8: Behaviour of core loss as a function of a) field strength, b) annealing temperature, c) frequency and d) cooling rate

From the above discussions, we concluded that the magnetic properties such as remanence, coercivity, peak permeability and core loss are highly structure sensitive and shows changes with change in the process parameters.

Sample B

Fig. 3.9 shows the X-ray diffraction patterns of sample B in unannealed condition and at 1100°C, 1120°C, 1140°C, 1150°C and 1180°C temperature respectively. From the diffraction patterns, we observed that an austenitic single phase Ni_3Fe is formed and the crystal structure is face centered cubic (FCC) and matched with the JCPDS card number 380419 [20-21]. However, little variation in the peak intensity is observed, which is due to the different annealing temperatures and also the domains are mostly aligned towards <200> direction. The effect of annealing temperature on the lattice parameter as a function of annealing temperature is given in Table 3.3, which shows that, there is not any significant change in the lattice parameter with increase in the annealing temperature.

Table 3.3: Variation of lattice parameter 'a' as a function of temperature

Temperature (°C)	**a (A^o)**
1100	3.550
1120	3.552
1140	3.554
1150	3.548
1160	3.550
1180	3.550

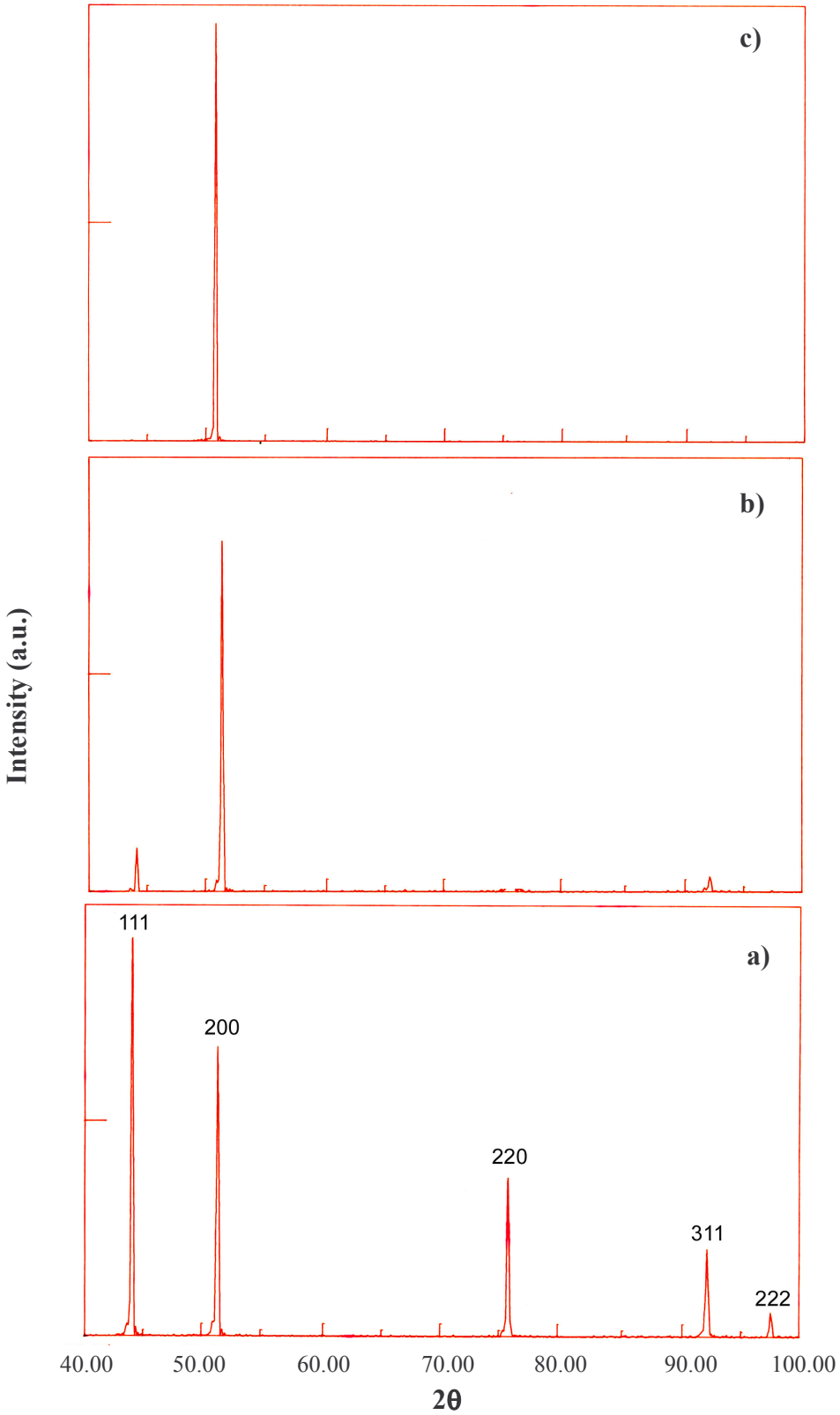

Fig. 3.9a: X-ray diffraction patterns of the sample B a) in unannealed condition, b) 1100°C and c) 1120°C

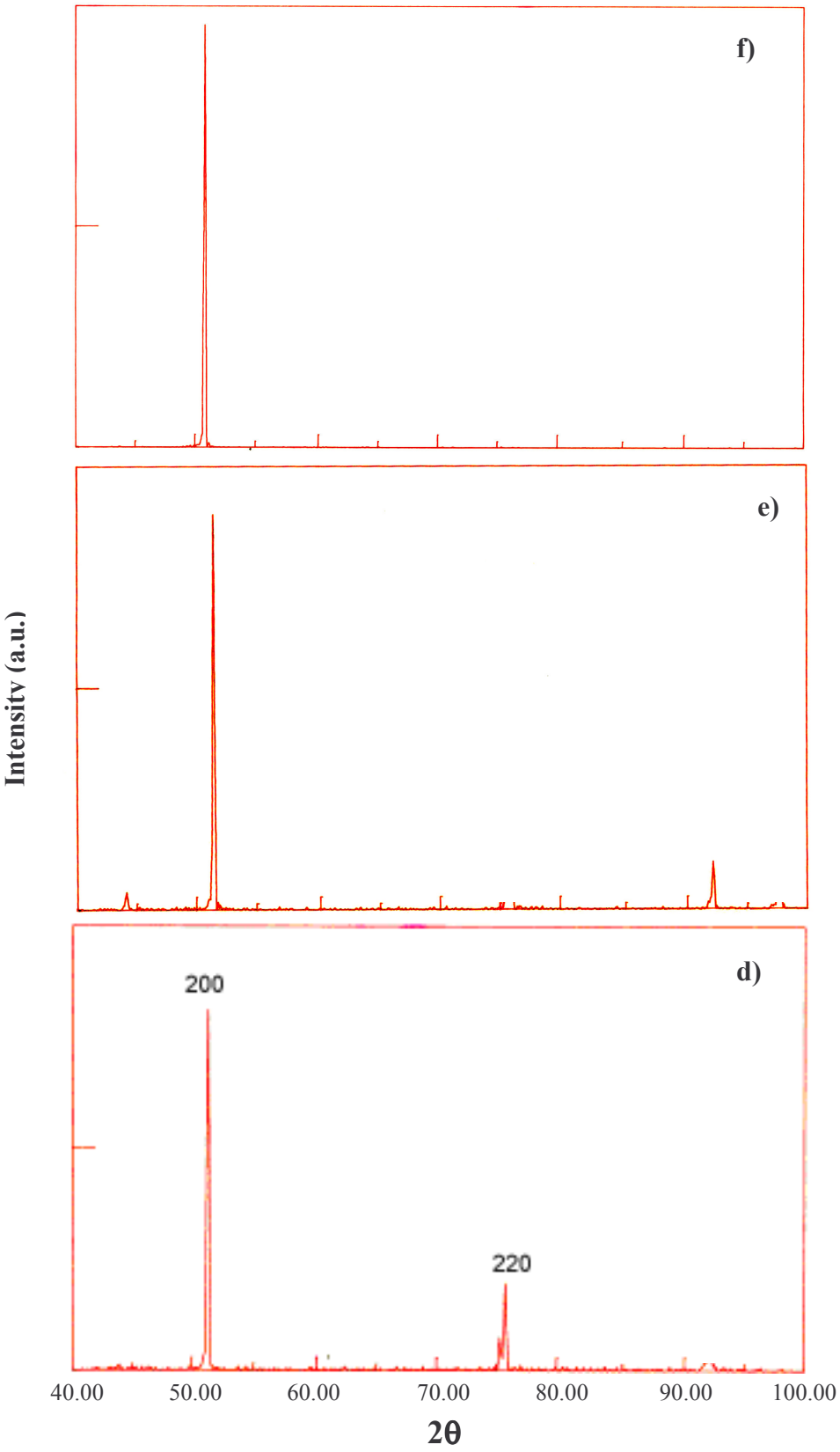

Fig. 3.9b: X-ray diffraction patterns of sample B at d) 1140°C, e) 1150°C and f) 1180°C

Fig. 3.10 shows the optical micrographs of sample B at 100X magnification after annealed at 1100°C, 1120°C, 1140°C, 1150°C, 1160°C and 1180°C respectively. We observed that with increase in the annealing temperature, the grain structure shows slight changes in the grain diameter. Also, in all the micrographs, twin boundaries appear at the grain boundaries. The average grain diameter observed in the sample B is 277 μm.

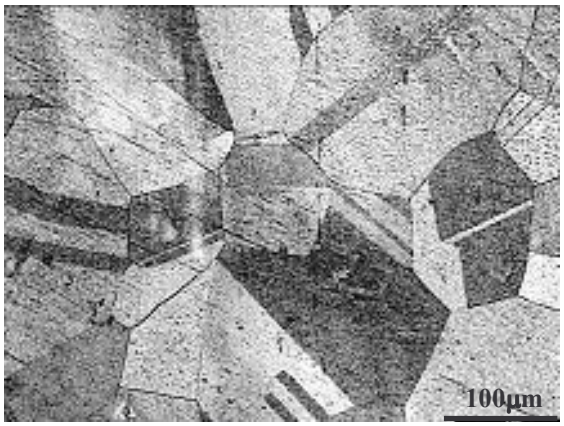

(a)

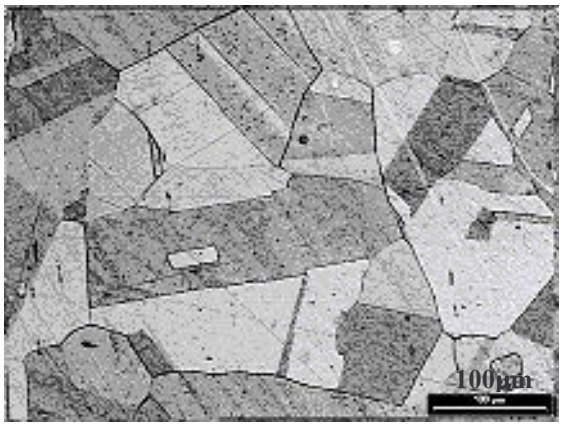

(b)

Fig. 3.10a: Optical micrographs of sample B at a) 1100°C and b) 1120°C

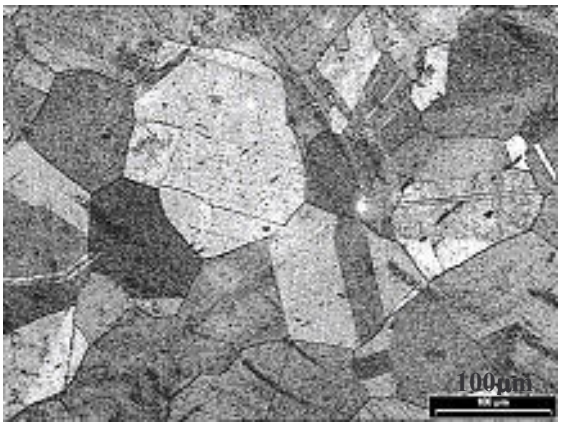

(c)

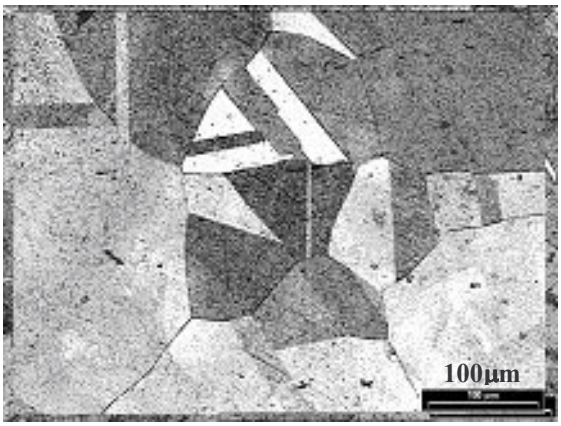

(d)

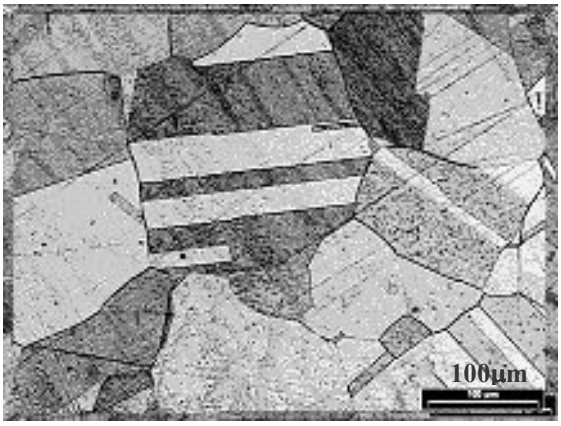

(e)

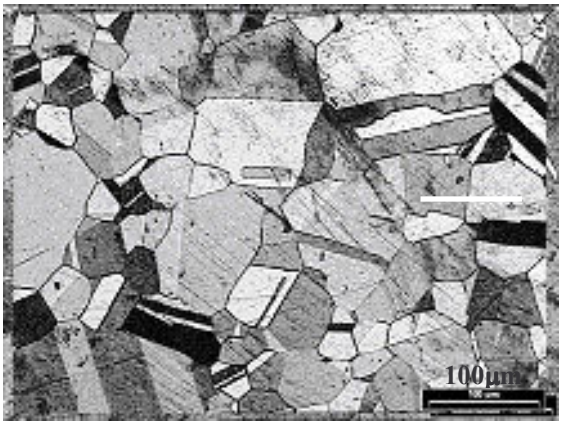

(f)

Fig. 3.10b: Optical micrographs of sample B at c) 1140°C, d) 1150°C, e) 1160°C and f) 1180°C

Table 3.4 shows the effect of the annealing temperature on the magnetic properties of sample B at 300 Hz [23-24].

Table 3.4: Effect of annealing temperature on magnetic properties

Annealing temperature (°C)	B_r (mT)	H_c (A/m)	Peak permeability	Core loss (mW)
1100	545.26	78.51	3000	10
1120	549.23	82.47	2947	11
1140	577.58	83.74	2996	11
1150	575.71	82.70	2950	11
1160	572.42	82.23	2972	11
1180	555.26	85.01	2930	11

Fig. 3.11 shows a typical behaviour of induction in sample B corresponding to a function of field strength. We observed that at input frequency of 300 Hz and at 1150°C temperature, induction increases exponentially from 737 mT to 748 mT as field strength increases from 200 A/m to 600 A/m and thereafter tends to saturate at 750 mT as the field strength further increases up to 900 A/m. Similar behaviour has been depicted at another temperatures as shown in Fig. 3.11.

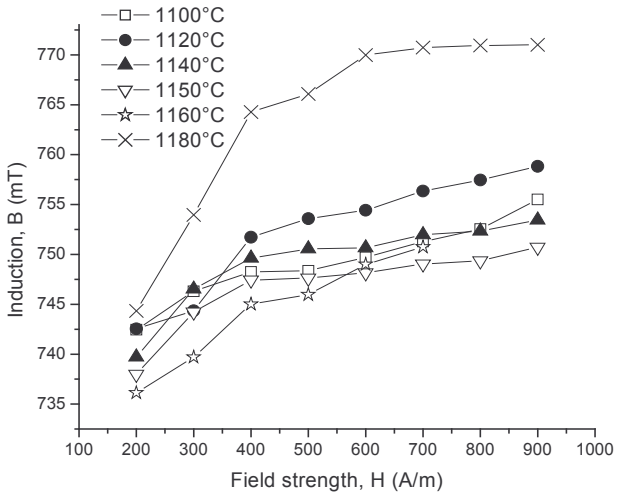

Fig. 3.11: Behaviour of induction as a function of field strength at 300 Hz

The behaviour of remanence in sample B corresponding to a function of field strength, annealing temperature, frequency and cooling rate is given in Fig. 3.12 (a-d) respectively. We observed that at a temperature of 1100°C, B_r decreases exponentially from 545 mT to 424 mT where field strength increases from 200 A/m to 900 A/m at 1100°C. Similar behaviour has been observed at all other temperatures as shown in Fig. 3.12a. The temperature dependence of B_r at an field strength of 200 A/m, shows an increase up to 1140°C thereafter decreases with increase in temperature up to 1180°C as shown in Fig. 3.12b. These results were reported at a constant cooling rate of 2.5°C/min. and holding time of 2 h. The behaviour of B_r is also studied as a function of frequency. We noticed that at a temperature of 1150°C, B_r increase from 424 mT to 575 mT with increase in the frequency from 100 Hz to 300 Hz. Similar behaviour has also been noticed at other studied temperatures as shown in Fig. 3.12c. The B_r shows an interesting behaviour as a function of cooling rate as shown in Fig. 3.12d. The remanence shows little variations in the lower cooling rate i.e. 2 to 3°C/min at field strength of 200 A/m thereafter increases with increase in the cooling rate. The similar behaviour has been reported for higher field strengths.

Fig. 3.13 (a-d) shows the behaviour of coercivity of sample B as a function of field strength, annealing temperature, frequency and cooling rate respectively. We observed that at an input frequency of 300 Hz and at a temperature of 1100°C, H_c increases from 78 A/m to 167 A/m where field strength increases from 200 A/m to 900 A/m. Similar behaviour has been depicted at another temperatures as shown in Fig. 3.13a. We also observed that the coercivity shows little variations with increase in the temperature from 1100°C to 1180°C as shown in Fig. 3.13b. We noticed that at a temperature of 1150°C, the coercivity increases from 55 A/m to 82 A/m with increase in frequency from 100 Hz to 300 Hz as given in Fig. 3.13c. Similar behaviour of coercivity has been noticed at other temperatures. The coercivity shows an interesting behaviour as a function of cooling rate as shown in Fig. 3.13d. We observed that H_c shows little variations at lower cooling rate i.e. 2 to 3°C/min. but almost stable at higher cooling rate and higher field strengths.

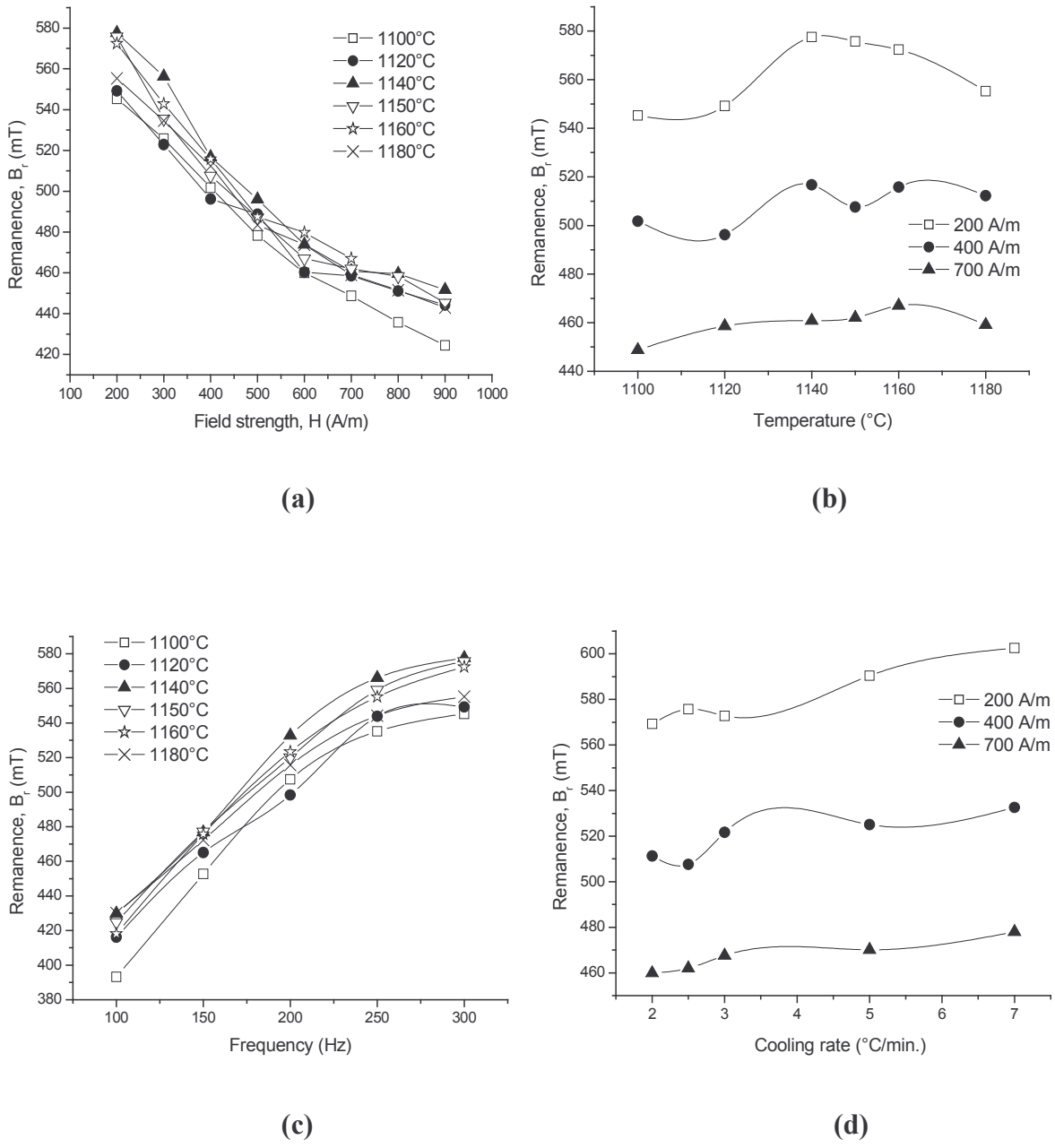

Fig. 3.12: Behaviour of remanence as a function of a) field strength, b) annealing temperature, c) frequency and d) cooling rate

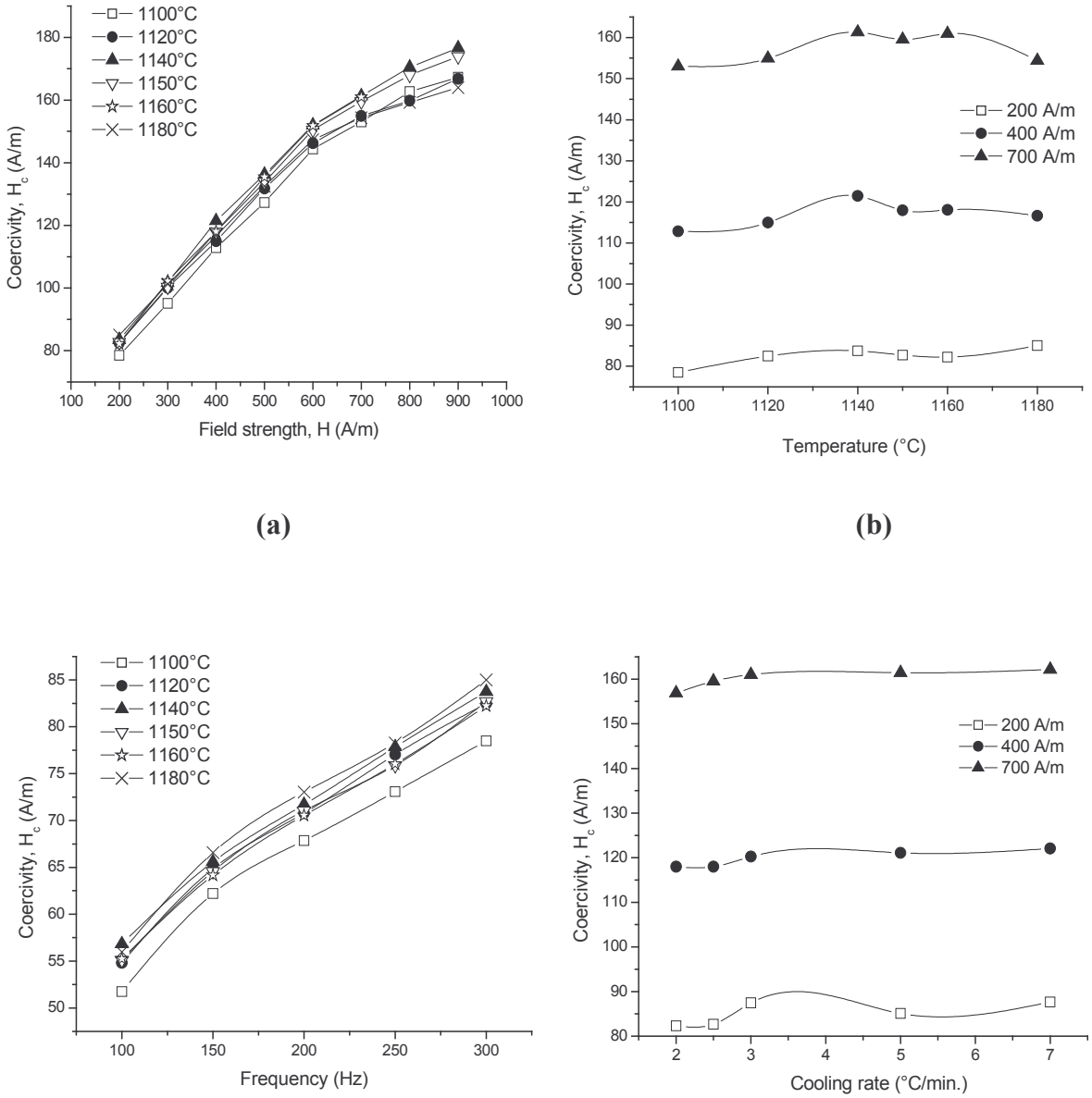

Fig. 3.13: Behaviour of coercivity as a function of a) field strength, b) annealing temperature, c) frequency and d) cooling rate

The behaviour of peak permeability as a function of field strength, annealing temperature, frequency and cooling rate is given in Fig. 3.14 (a-d) respectively. We noticed that at a input frequency of 300 Hz and at a temperature of 1150°C, the peak permeability decreases exponentially from 2950 to 667 where the field strength increases from 200 A/m to 900 A/m. Similar behaviour has been depicted at other temperatures as shown in Fig. 3.14a. The temperature dependence of peak permeability shows little variations at lower field strength of 200 A/m and at input frequency of 300 Hz but shows stability at higher field strengths i.e. 400 A/m and 700 A/m as shown in Fig. 3.14b. We observed that at 1100°C temperature, the peak permeability decreases from 10996 to 3000 with increase in the frequency from 100 Hz to 300 Hz. Similar behaviour of peak permeability has been noticed at other temperatures as shown in Fig. 3.14c. We also noticed that at a field strength of 200 A/m, the peak permeability shows little variations at lower cooling rate i.e. 2 to 3°C/min. and shows stability at higher cooling rate i.e. 7°C/min. as shown in Fig. 3.14d. Similar effect has been seen at other higher field strengths i.e. 400 A/m and 700 A/m.

An interesting behaviour of core loss as a function of field strength, annealing temperature, frequency and cooling rate is given in Fig. 3.15 (a-d) respectively. We observed that at 300 Hz and at a temperature of 1100°C, the core loss increases from 10 mW to 27 mW with increase in field strength from 200 A/m to 900 A/m (Fig. 3.15a). The temperature dependence of core loss shows stability at lower field strength of 200 A/m and shows little variations at higher field strength as shown in Fig. 3.15b. This may be due to the localized heating effect of the material at such higher field strength. The core loss as function of frequency increases from 2 mW to 11 mW with increase in the frequency form 100 Hz to 300 Hz for all studied temperatures (Fig. 3.15c). This satisfies the equation 3.3. Also, we observed that the core loss increases when the cooling rate increases from 2 to 3°C/min. thereafter it decreases with further increase in the cooling rate up to 5°C/min. and again increases with further increase in the cooling rate to 7°C/min at all the field strength as shown in Fig. 3.15d.

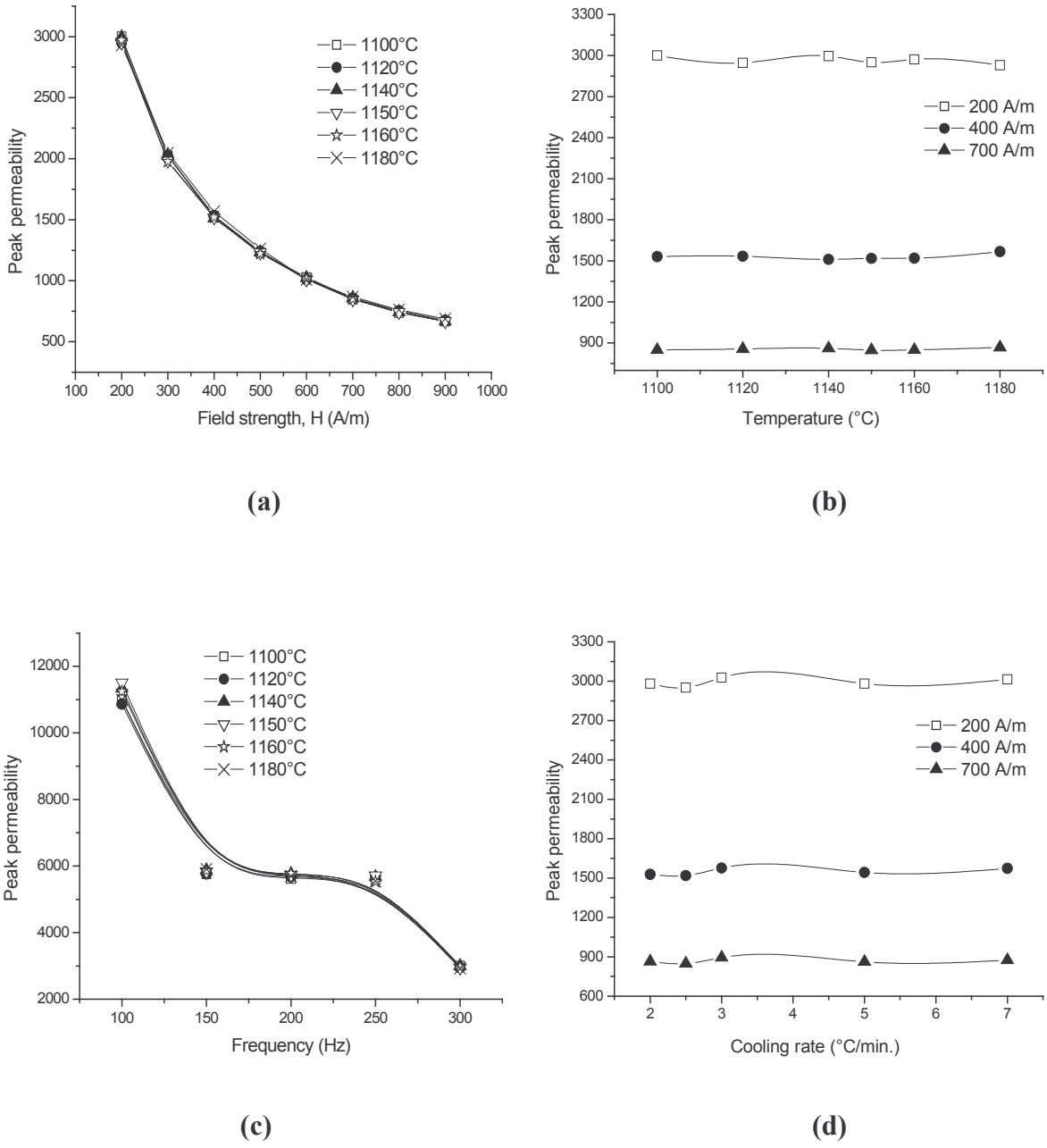

Fig. 3.14: Behaviour of peak permeability as a function of a) field strength, b) annealing temperature, c) frequency and d) cooling rate

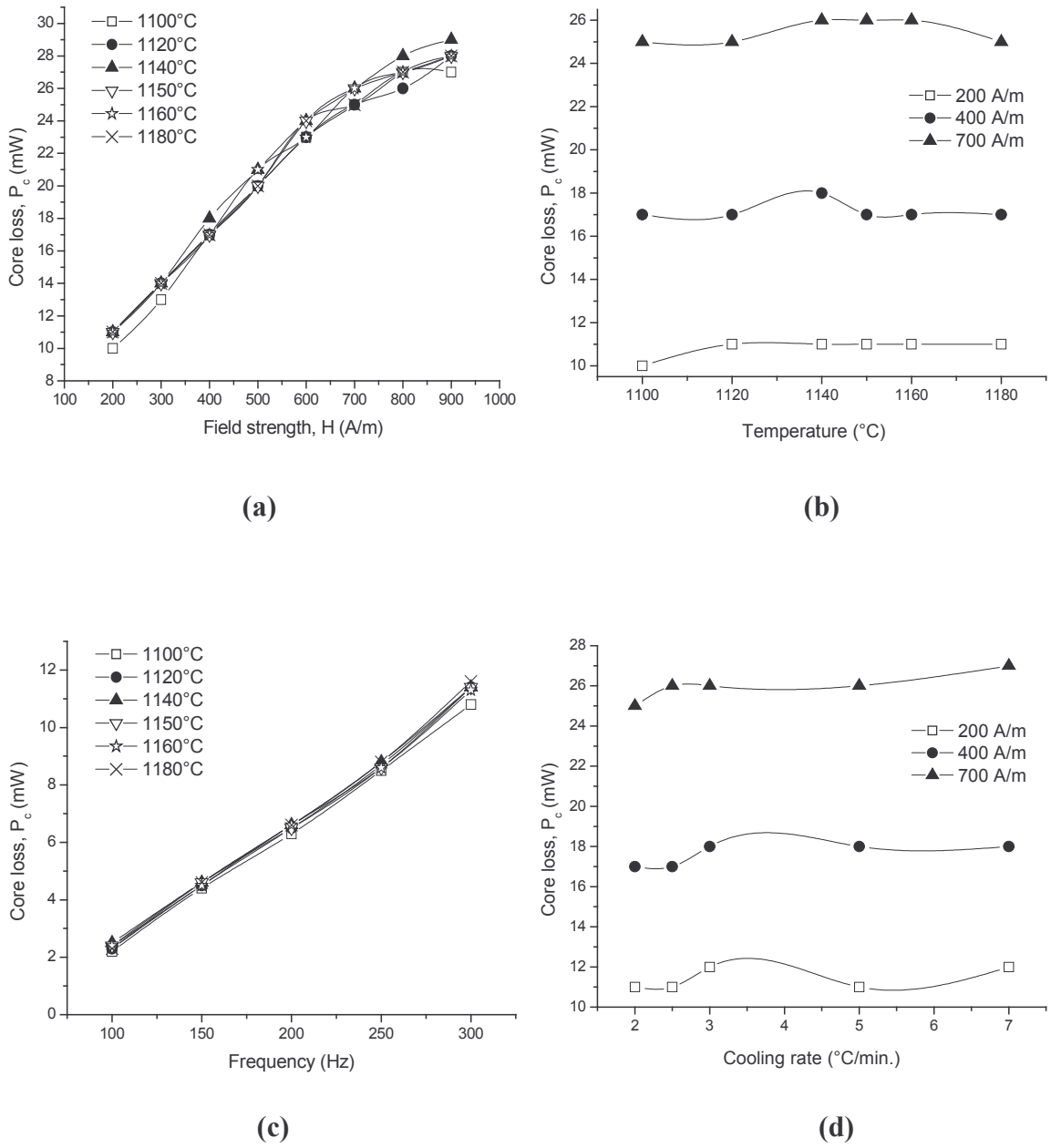

Fig. 3.15: Behaviour of core loss as a function of a) field strength, b) annealing temperature, c) frequency d) cooling rate

Sample C

Fig. 3.16 shows the X-ray diffraction patterns of sample C in unannealed condition and at 1100°C, 1120°C, 1140°C, 1150°C and 1180°C temperature respectively. From the diffraction patterns, we noticed that a austenitic single phase γ-[Fe, Ni] is formed and the crystal structure is face centered cubic (FCC), matched with the JCPDS card number 471417 [20-21]. However, little variation in the peak intensity is observed, which is due to the different annealing temperatures and also the domains are mostly aligned towards <200> direction. The effect of annealing temperature on lattice parameter is given in Table 3.5. Slight variations were observed in the lattice parameter with increase in the annealing temperature.

Table 3.5: Variation of the lattice parameter 'a' as a function of temperature

Temperature (°C)	**a (A^0)**
1100	3.594
1120	3.594
1140	3.588
1150	3.586
1160	3.586
1180	3.588

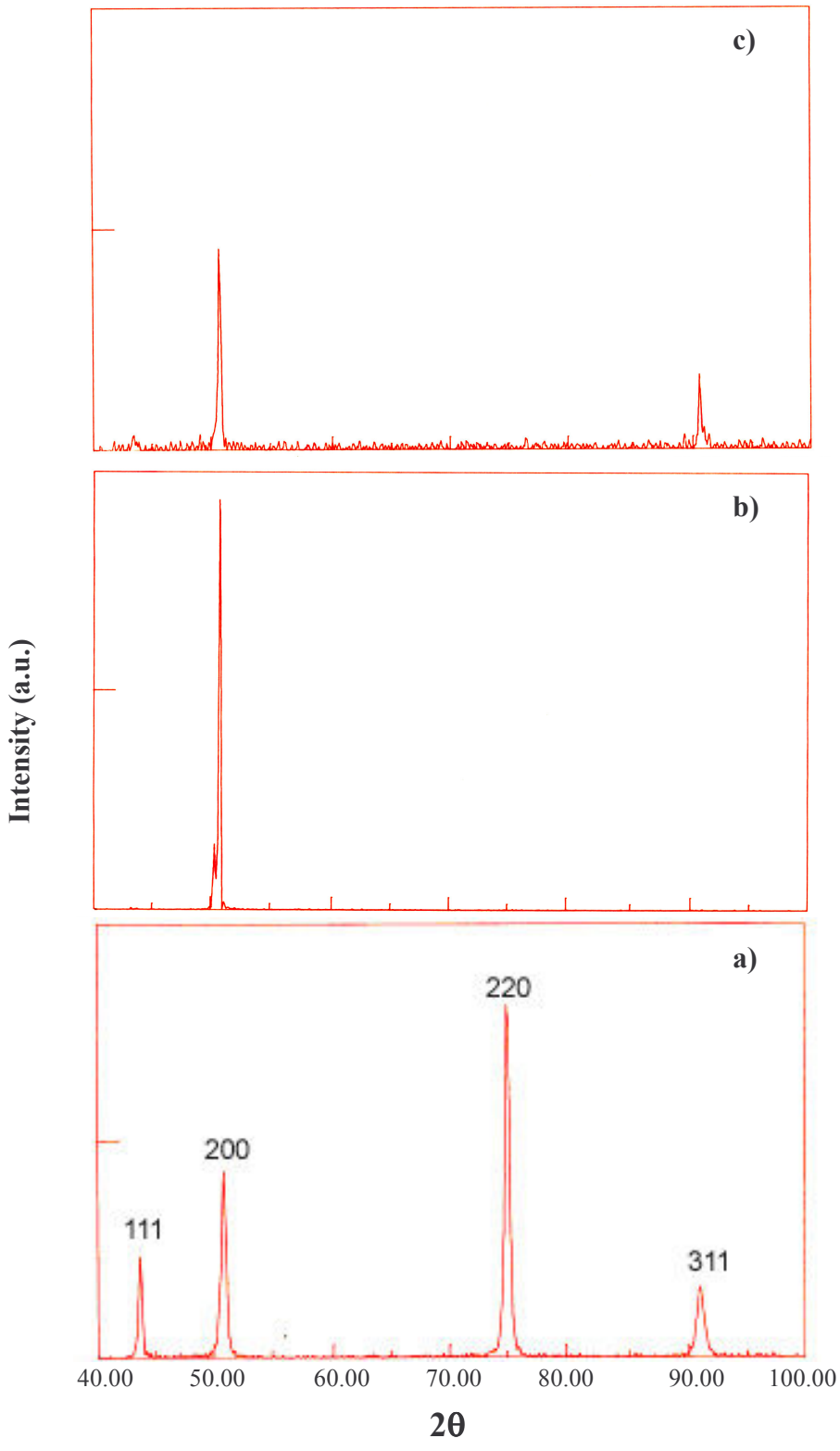

Fig. 3.16a: X-ray diffraction patterns of sample C a) in unannealed condition, b) 1100°C and c) 1120°C

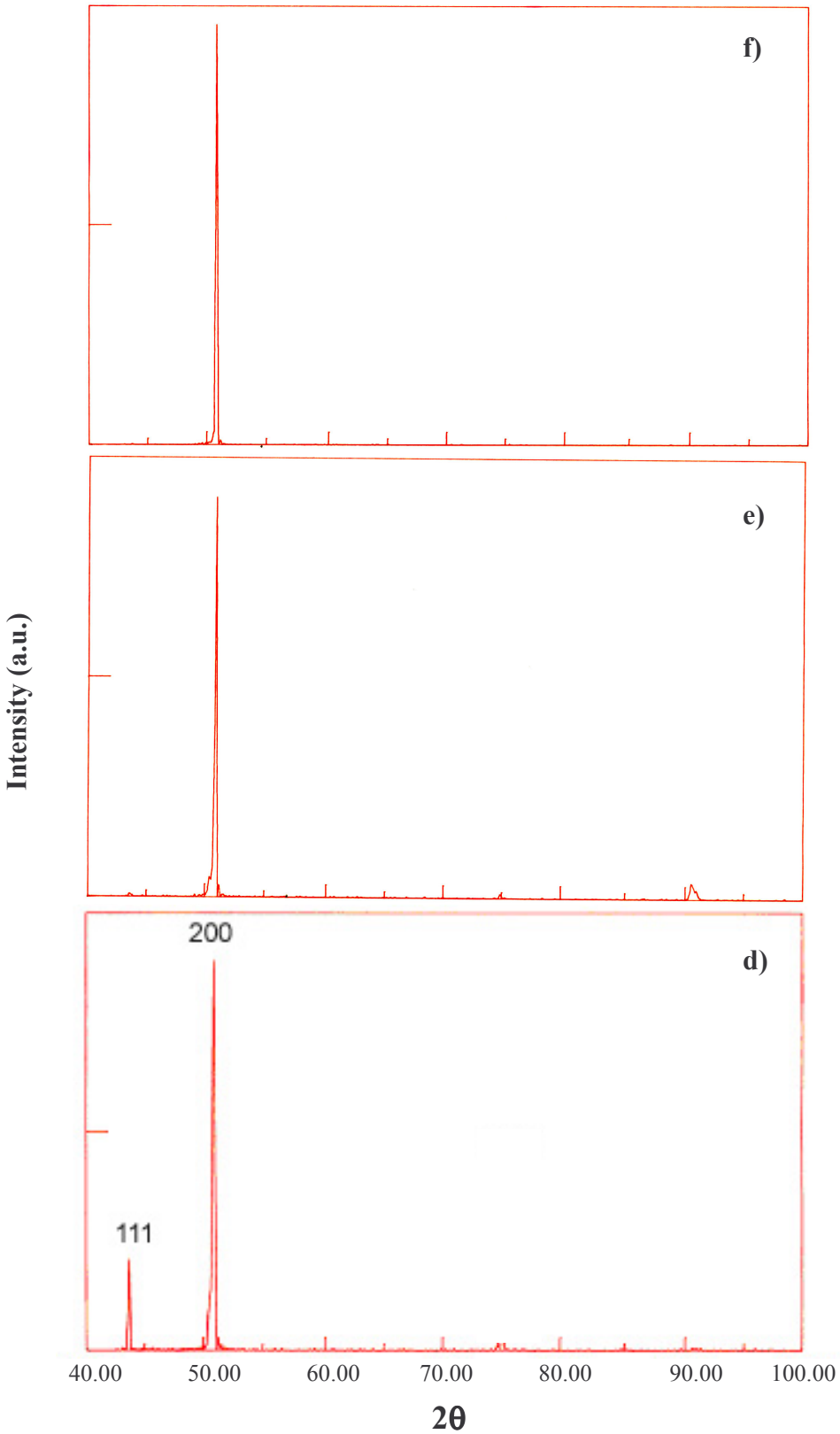

Fig. 3.16b: X-ray diffraction patterns of sample C at d) 1150°C, e) 1160°C and f) 1180°C

Fig. 3.17 shows the optical micrographs of sample C at 100X magnification after annealed at 1100°C, 1120°C, 1140°C, 1150°C, 1160°C and 1180°C respectively. The micrographs shows that with increase in the annealing temperature, grain diameter slightly increases but it does not have significant effect on the magnetic properties as explained in the next chapter. Also, in all the micrographs, twin boundaries appear at the grain boundaries. The average grain diameter observed in the sample C is 127 μm.

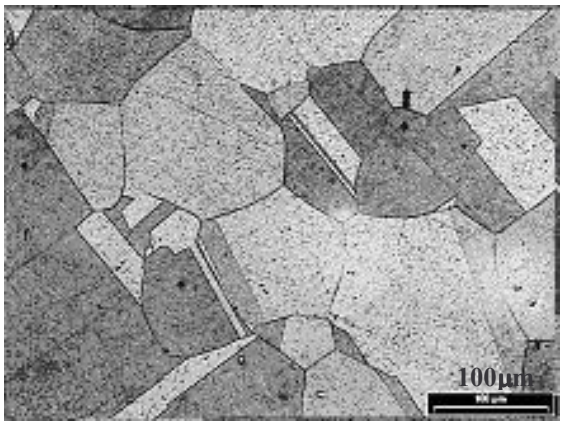

(a)

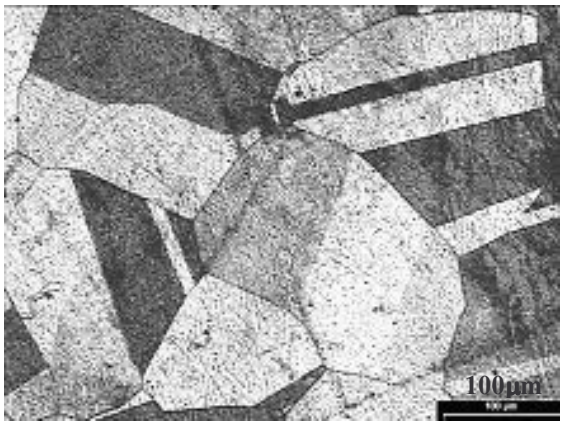

(b)

Fig. 3.17a: Optical micrographs of sample C at a) 1100°C and b) 1120°C

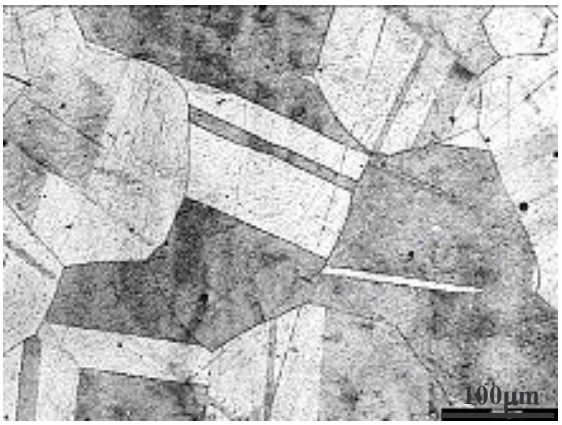

(c)

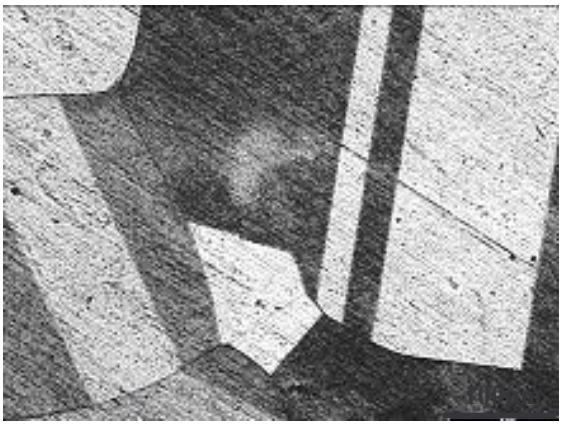

(d)

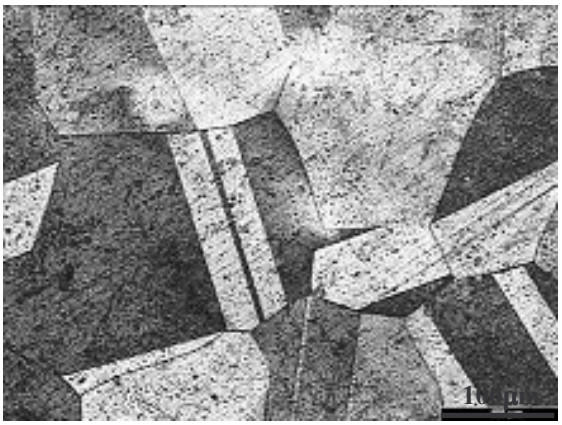

(e)

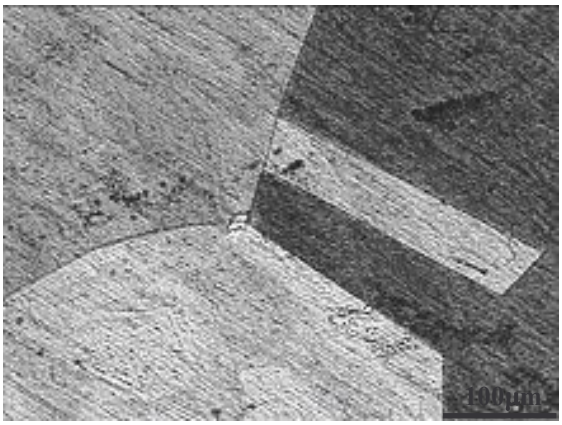

(f)

Fig. 3.17b: Optical micrographs of sample C at c) 1140°C, d) 1150°C, e) 1160°C and f) 1180°C

Table 3.6 shows the magnetic properties of sample C as a function of annealing temperature [23-25].

Table 3.6: Effect of annealing temperature on magnetic properties

Annealing temperature (°C)	B_r (mT)	H_c (A/m)	Peak permeability	Core loss (mW)
1100	1173.10	255.78	2370	59
1120	1088.86	245.69	2394	56
1140	1175.28	251.96	2376	59
1150	1182.63	256.25	2364	59
1160	1177.19	254.41	2390	59
1180	1107.15	249.38	2395	58

A typical behaviour of induction in sample C corresponding to a function of field strength is given in Fig. 3.18. We observed that at input frequency of 300 Hz and at 1150°C, induction increases exponentially from 1492 mT to about 1621 mT as field strength increases from 500 A/m to 1400 A/m and thereafter tends to saturate at 1629 mT as field strength further increases to 1600 A/m. Similar behaviour has been depicted at another temperatures as shown in Fig. 3.18.

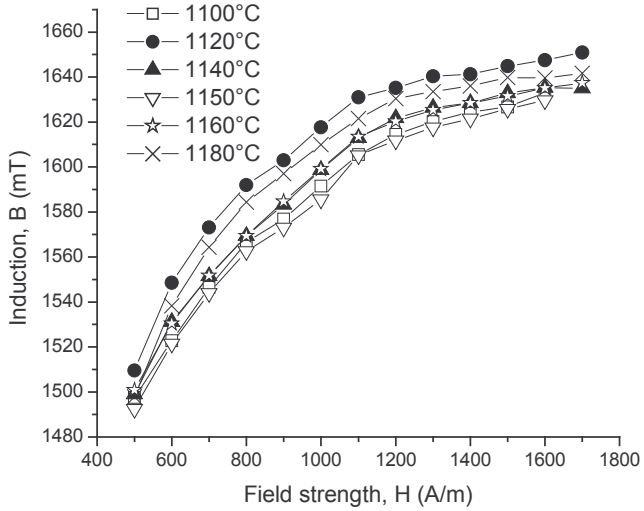

Fig. 3.18: Behaviour of induction as a function of field strength at 300 Hz

The behaviour of remanence in sample C corresponding to a function of field strength, annealing temperature, frequency and cooling rate is given in Fig. 3.19 (a-d) respectively. We observed that at an input frequency of 300 Hz, B_r decreases from 1182 mT to 1027 mT where field strength increases from 500 A/m to 1600 A/m at 1150°C. Similar behaviour has been depicted at another temperatures as shown in Fig. 3.19a. The remanence decreases from 1173 mT to 1088 mT with increase in the annealing temperature from 1100 to 1120°C at an field strength of 500 A/m and thereafter increases to 1182 mT with further increase in the temperature to 1150°C and decrease thereafter to 1107 mT with further increase in the temperature to 1180°C as shown in Fig. 3.19b. Similar behaviour has been seen at other higher field strengths. These results were reported at a constant cooling rate of 2.5°C/min. and holding time of 2 h. It is due to the change in the cell dimensions of the sample during annealing at different temperatures. The behaviour of B_r as a function of frequency is shown in Fig. 3.19c. We noticed that at a temperature of 1100°C, B_r increases exponentially from 970 mT to 1182 mT with increase in the frequency from 100 Hz to 300 Hz. Similar behaviour has been noticed at other studied temperatures. Also, B_r shows an interesting behaviour as a function of cooling rate as shown in Fig. 3.19d. The remanence initially increases and then decreases with increase in the cooling rate from 2 to 3°C/min at field strength of 500 A/m thereafter increases with increase in the cooling rate to 5°C/min. The similar behaviour has also been seen for other higher field strengths.

The behaviour of coercivity of sample C as a function of field strength, annealing temperature, frequency and cooling rate is given in Fig. 3.20 (a-d) respectively. We observed that at an input frequency of 300 Hz and at a temperature of 1100°C, H_c increases from 225 A/m to 449 A/m where field strength increases from 500 A/m to 1600 A/m. Similar behaviour has been depicted at other temperatures as shown in Fig. 3.20a. An interesting behaviour of coercivity as a function of annealing temperature at 300 Hz frequency is shown in Fig. 3.20b. We observed that at field strength of 500 A/m, the coercivity shows variations in the intermediate temperature range of 1140-1160°C where as it remains nearly stable at the other temperatures. Similar behaviour has been seen at other higher field strengths. From Fig. 3.20c, we noticed that at a temperature of 1100°C,

the coercivity increases from 165 A/m to 255 A/m with increase in frequency from 100 Hz to 300 Hz. Similar behaviour of coercivity has been noticed at other temperatures. We also observed that at field strength of 500A/m, the H_c shows variations under the lower cooling rate ranges from 2 to 3°C/min and becomes almost stable at the higher cooling rates as shown in Fig. 3.20d. Similar behaviour has been observed at other higher field strengths.

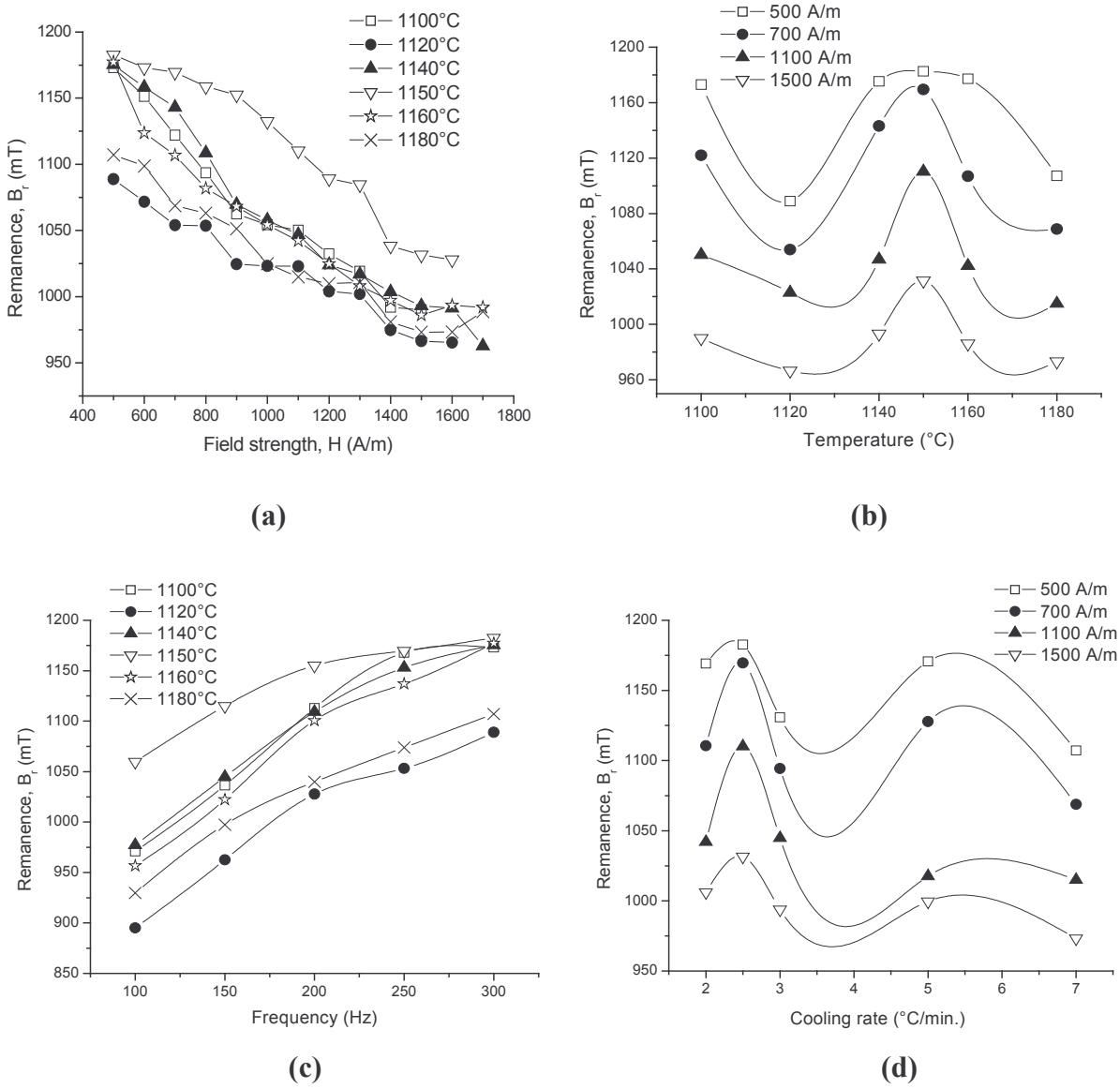

Fig. 3.19: Behaviour of remanence as a function of a) field strength, b) annealing temperature, c) frequency and d) cooling rate

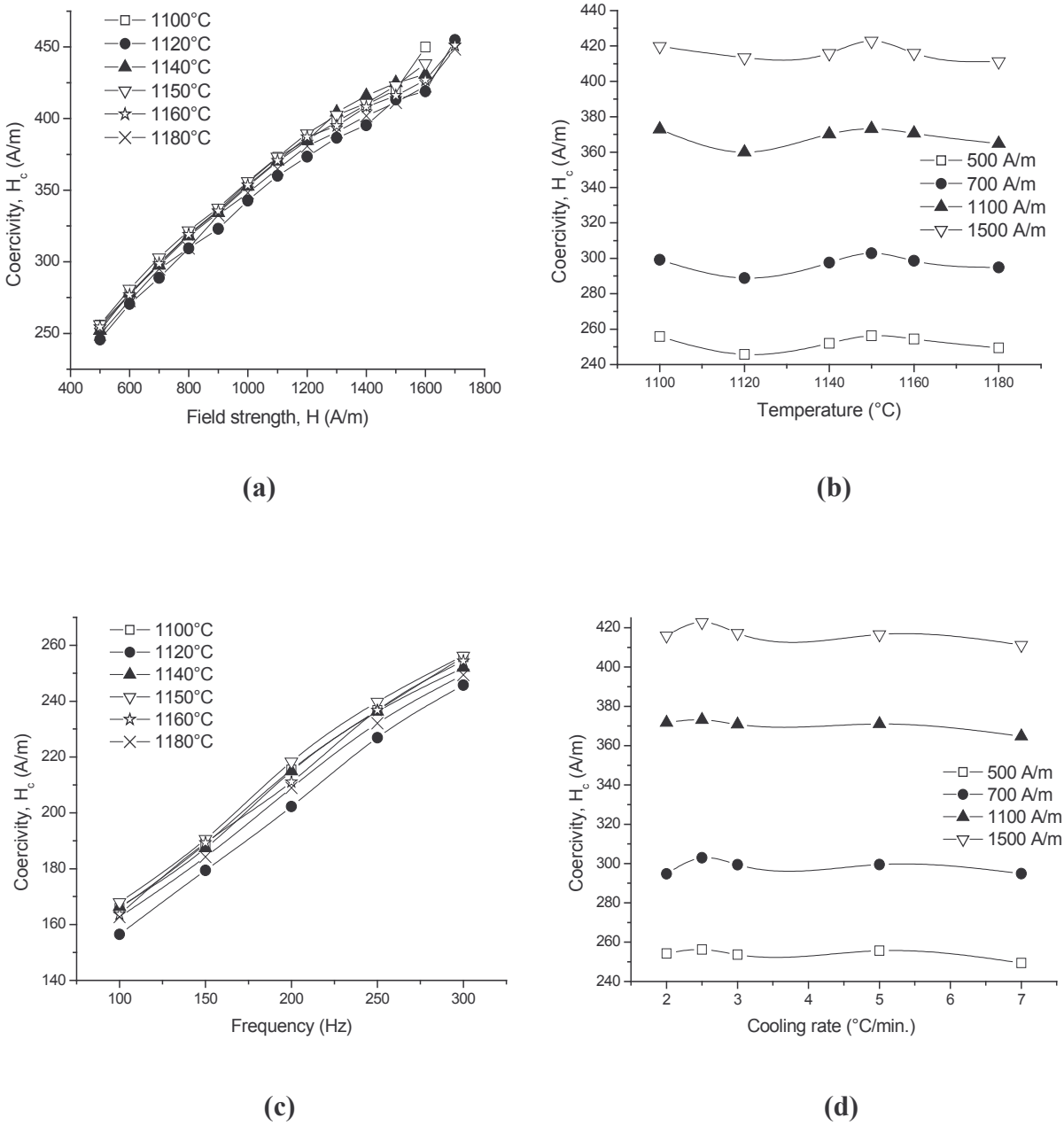

Fig. 3.20: Behaviour of coercivity as a function of a) field strength, b) annealing temperature, c) frequency and d) cooling rate

The behaviour of peak permeability as a function of field strength, annealing temperature, frequency and cooling rate is given in Fig. 3.21 (a-d) respectively. We observed that at a input frequency of 300 Hz and at a temperature of 1150°C, the peak permeability decreases exponentially from 2364 to 804 where the field strength increases from 500 A/m to 1700 A/m. Similar behaviour has been depicted at other temperatures as shown in Fig. 3.21a. The temperature dependence of peak permeability shows its stable behaviour at all field strengths as shown in Fig. 3.21b. The frequency dependence of peak permeability is given in Fig. 3.21c. We observed that at 1100°C temperature, the peak permeability decreases from 5429 to 2370 with increase in the frequency from 100 Hz to 300 Hz. Similar behaviour of peak permeability has been noticed at other temperatures. Also, we noticed that the peak permeability is almost stable as function of cooling rate as shown in Fig. 3.21d. But it shows slight variations at lower field strength i.e. 500 A/m and at lower cooling rate i.e. 2 to 3°C/min.

Fig. 3.22 (a-d) shows an interesting behaviour of core loss as a function of field strength, annealing temperature, frequency and cooling rate respectively. We observed that at 300 Hz and at a temperature of 1100°C, the core loss increases from 59 mW to 127 mW with increase in field strength from 500 A/m to 1700 A/m (Fig. 3.22a). The temperature dependence of core loss shows little variations in the temperature range of 1100 to 1140°C and thereafter shows stability with further increase in the temperature to 1180°C for all the field strengths as shown in Fig. 3.22b. The core loss as function of frequency increases from 12 mW to 59 mW with increase in the frequency form 100 Hz to 300 Hz for all studied temperatures (Fig. 3.22c). This also satisfies the equation 3.3. Also, we observed that the core loss shows small variations with increase in the cooling rate from 2 to 7 °C/min for all studied field strengths as shown in Fig. 3.22d.

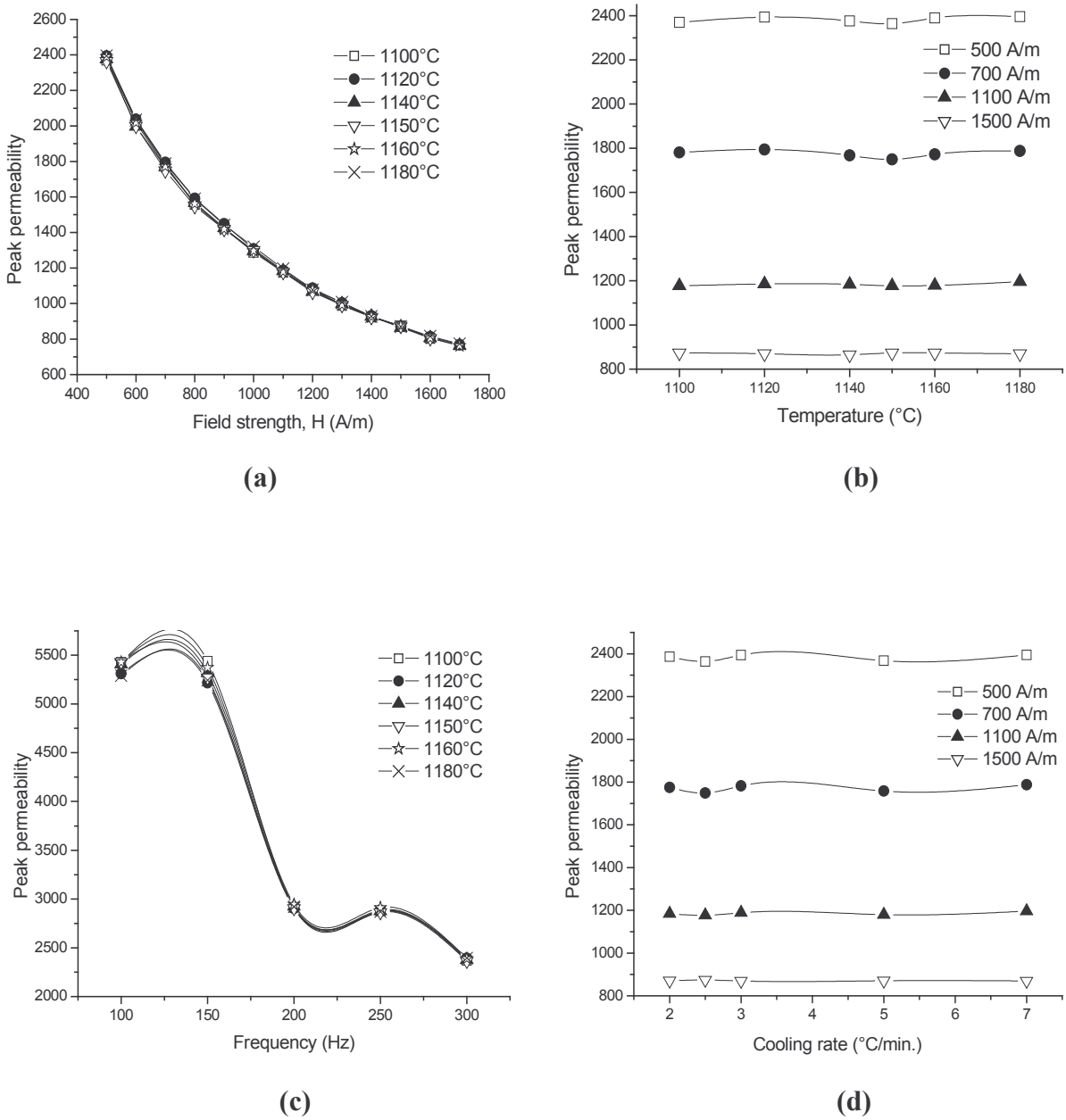

Fig. 3.21: Behaviour of peak permeability as a function of a) field strength, b) annealing temperature, c) frequency and d) cooling rate

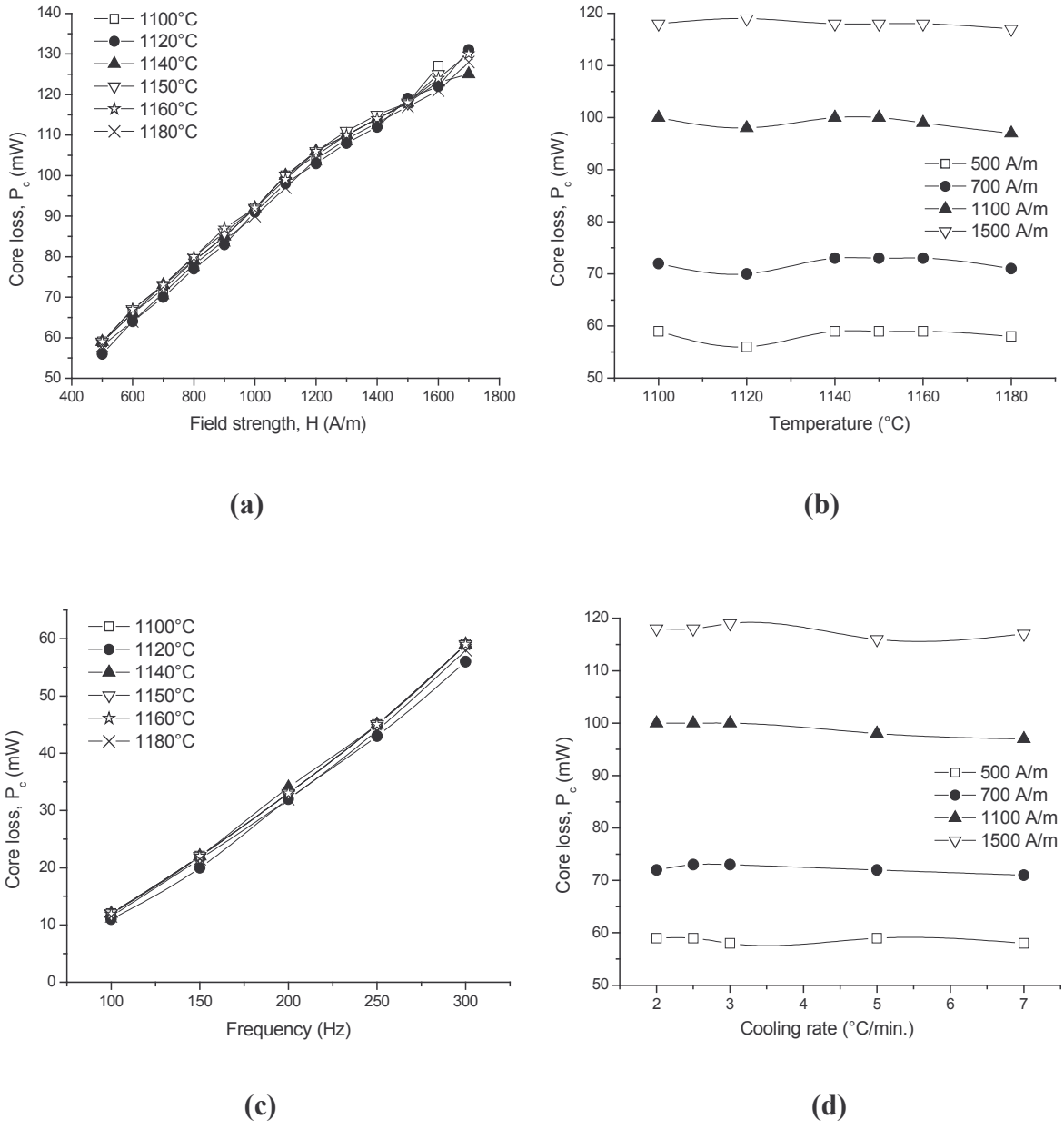

Fig. 3.22: Behaviour of core loss as a function of a) field strength, b) annealing temperature, c) frequency and d) cooling rate

3.3 Influence of annealing atmosphere on magnetic properties of sample A

Sample A was annealed in the presence of two different atmospheres such as H_2 and NH_3 and studied the magnetic properties under the changed atmosphere. Fig. 3.23 shows the effect of annealing atmosphere on the magnetic properties of sample A. It is evident from the Fig. 3.23a that the induction remains almost same when the sample is annealed in changed atmosphere. However, the remanence of sample A is less 413 mT in H_2 atmosphere where as it is 463 mT when annealed in NH_3 at field strength of 50 A/m and 100 Hz as shown in Fig. 3.23b. Whereas other magnetic properties such as coercivity, peak permeability and core loss show similar behaviour as a function of field strength when annealed in two different atmospheres as shown in Fig. 3.23 (c-e) respectively. This is due to that atmosphere used in the annealing whether it is H_2 or NH_3, is having dew point better than -50°C. Therefore, due to the lower the dew point in the furnace atmosphere, environment in the furnace is more reducing and therefore the surface properties of the end product are better. So, out of these two, any atmosphere can be used for the annealing of permalloy samples but the due point should be better than -50°C. Similarly, the magnetic properties of samples B and C were studied in the changed atmosphere conditions, but because similar behaviour has been observed in both the samples as in sample A, the data is not reported here.

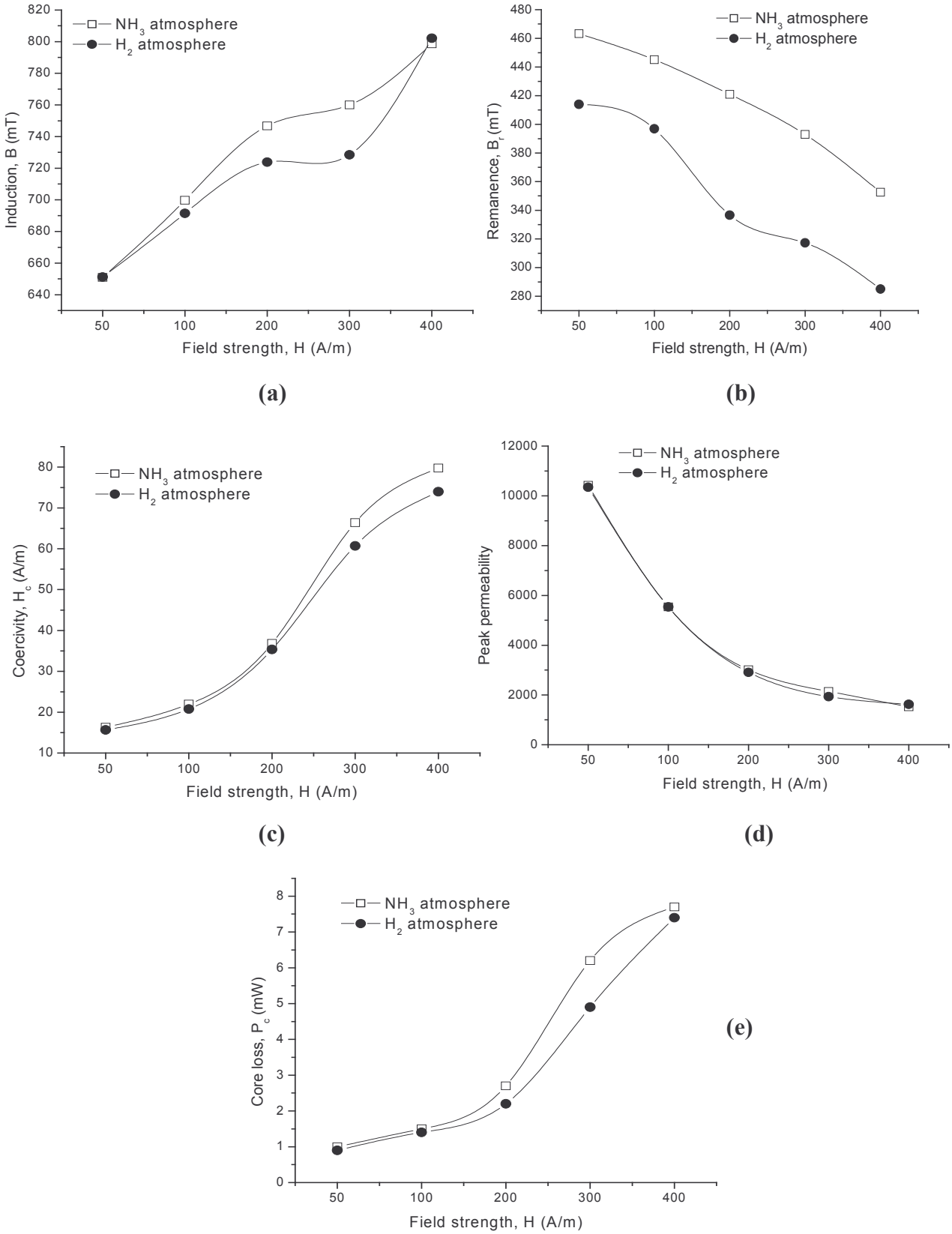

Fig. 3.23: Influence of annealing atmosphere on the magnetic properties of sample A

References

1. A. T. English & G. Y. Chin, J. Appl. Phys., **38** (1967) 1183
2. H. H. Scholefield, R.V. Major, B. Gibson & A. P. Martin, Brit. J. Appl. Phys., **18** (1967) 41
3. R. D. Enoch & A. D. Fudge, Brit. J. Appl. Phys., **17** (1966) 623
4. ASM Handbook : Metallography and Microstructures (ASM Internationals, USA) **9** (1995) 538
5. T. Akomolafe & G. W. Johnson, J. Appl. Phys., **24** (1989) 349
6. D. W. Dietrich, ASM Handbook: Magnetically Soft Materials, Properties and Selection : Non-ferrous alloys and special purpose materials, ASM Internationals, NY, **2** (1990) 761
7. G. Y. Chin, IEEE Trans. Magn., **7** (1971) 102
8. R. M. Bozorth, Ferromagnetism (D van Nostrand Company Inc., New York, London, Toronto), 1951
9. F. Pfeifer & C. Radeloff, J. Magn. Magn. Mater., **19** (1980) 190
10. F. Pfeifer, Encyclo. Mater. Sci. Engg., **4** (1986) 2663
11. Li Lin & M. S. Masteller, IEEE Trans Magn., **33** (1997) 3769
12. G. Couderchon & J. F. Tiers, J. Magn. Magn. Mater., **26** (1982) 196
13. Li Lin, IEEE Trans Magn., **37** (2001) 2315
14. R. N. P Choudhary & P. K. Sinha, Mater Sci Engg., **B 98** (2003) 74
15. K.Varatharajan & A.K.Tyagi, Pract. Metallo. **35** (1998) 1
16. Instruction Manual, Automatic Hysteresisgraph, AMH-401, Walker Scientific Inc., USA, 1997
17. Data Sheet No. 9002, Magnifer 50, Thyssenkrupp V D M, 2002
18. Special Quality Manual, Sankyo Standards, Japan **4** (1998)
19. Datasheet No. 9004, Magnifer 7904, Krupp V D M, 2000
20. JCPDS-International Centre for Diffraction Data, PCPDFWIN, **2.02** (1999)
21. B. D. Cullity, Elements of X-ray diffraction, 3rd ed., Prentice –Hall, Upper Saddle River, N J, 2001
22. Kiran Gupta, K. K. Raina & S. K. Sinha, Ind. J. Engg. Mater. Sci., **12** (2005) 577

23. Kiran Gupta, S. K. Sinha & K. K. Raina, Proc. nat. conf. on materials for electrical, electronic & magnetic applications: Characterisation & measurements, Hyderabad DMRL, (2005) 6B.5
24. Kiran Gupta, K. K. Raina & S. K. Sinha, Bull. Mater. Sci., **29** (2006) 391
25. Kiran Gupta, S. K. Sinha & K. K. Raina, Proc. nat. conf. on advances in condensed matter physics, Patiala TIET, (2005) 11